Direct simulations of the stress redistribution in the scaling organization of fracture tectonics (SOFT) model

C. Narteau,[1] P. Shebalin,[1,2] M. Holschneider,[3] J.-L. Le Mouël[1] and C. J. Allègre[1,4]

[1] *Institut de Physique du Globe de Paris,* 4, *Place Jussieu, Paris, Cedex* 05, 75252, *France.* E-mail: narteau.ipgp.jussieu.fr
[2] *International Institute of Earthquake Prediction Theory and Mathematical Geophysics, Warshavskoye shosse,* 79, *korp* 2, *Moscow* 113556, *Russia*
[3] *Centre de Physique Théorique, CNRS, Case* 907, F-13288 *Marseille, France*
[4] *Université Paris* VII, 4, *Place Jussieu,* 75252 *Paris Cedex* 05, *France*

SUMMARY
A time-dependent stochastic process with three states (solid, broken and moving) is considered in a hierarchical system made of embedded cells of increasing levels. An earthquake of a given scale k is associated with the moving state of a cell of level k and results from the coherent self-organization of fractures of lower scales. A direct cascade of stress redistribution generates small-scale stress heterogeneities in the neighbourhood of the active fracture. An interesting feature of the model is that the size of the domain where stress redistribution takes place grows proportional to the length of the fracture. In the framework of the general model, inspired by the progress in the use of the renormalization techniques in approaching critical point phenomena, we independently study a 'fracturing' submodel and a 'friction' submodel. These submodels are two-state models that act on different timescales. In the 'friction' submodel, which comprises broken and moving states, the transitions between these two states are associated with stick–slip behaviour in a completely fractured fault zone. In the 'fracturing' submodel, which comprises solid and broken states, we model the brittle behaviour of rock material. In both models we obtain a spatio-temporal clustering of earthquakes, realistic aftershock sequences whose frequency decreases respect the modified Omori law, and a frequency–magnitude relationship that respects the Gutenberg–Richter law. We show that the model behaviour is controlled by the stress heterogeneity in the fault zone, we find evidence for a relationship between the periodicity of the largest earthquakes and the b-value, and we indicate how the different physical ingredients underlying each submodel can be gathered together in a more general model.

Key words: cascade, heterogeneity, hierarchical system, Omori law, seismicity.

1 INTRODUCTION

Earthquakes mainly occur in fault zones—boundaries between tectonic plates—and result from the relative large-scale motions of these plates. These fault zones include a large number of faults that interact together (Harris 1998) to accommodate the large-scale deformation. Most faults are schematically characterized by two phases during their history: an aseismic long time period, without relative motion of the two sides of the fault, separated by short periods of seismic activity (foreshocks–main shock–aftershocks sequence, swarm of small earthquakes). Other faults produce aseismic slip (slow earthquakes, creep) with a large number of microearthquakes. Information collected has revealed a spatio-temporal cluster-

ing of the seismicity and various types of statistical behaviour such as the Gutenberg–Richter power law concerning the size–frequency statistics [Gutenberg & Richter (1994), who noted that 'earthquakes may be expected to occur in the future, as in the past'], the Omori law, which describes the aftershock frequency decrease (Omori 1894; Utsu *et al.* 1995) as well as the foreshock frequency increase (Papazachos 1975), and the relation between the energy radiated by an earthquake and its size (Kanamori & Anderson 1975).

The fracturing process determines the length of the major fault as well as the distribution of cracks at all scales. Friction can then play its part in the fractured zone. The development of a constitutive law of rock friction (Dieterich 1979) has provided a frictional interpretation of a large range of deformation

phenomena (Scholz 1998) associated with pre-existing fractures: creep (Scholz 1990), seismic regimes (Marrone & Scholz 1988; Tse & Rice 1986), aftershocks (Dieterich 1994), nucleation phases (Campillo & Ionescu 1997), seismic cycles (Ben-Zion 1996; Rice & Ben-Zion 1996) and coseismic phases (Cochard & Madariaga 1994). Nevertheless, shear fractures do not always occur along pre-existing structures and the rupture could be initiated in or propagate into intact or healed bulk rock. For long time periods, and to include the large-scale heterogeneity of rheological rock properties, the analysis of the rupture of a fault zone has to include the fracture mechanism (Yamashita & Ohnaka 1991).

Earthquake genesis can also be tackled with tools of non-linear physics (e.g. Dubois & Gvishiani 1998). The seismogenic layer of the Earth has been considered to exhibit a state of 'self-organized criticality' (SOC) (Bak & Tang 1989; Main 1997). A large number of phenomenological models (see references in Main 1996) reproduce this statistically stationary state characterized by spatial and temporal correlation functions with a power-law behaviour. This was also obtained by Correig *et al.* (1997), who used a cellular automaton to model the aftershock frequency decrease. Discarding the state of SOC, Knopoff (1997) suggested that the healing of cracks and the rate of healing have to be taken into account in a fault zone (Marrone 1998) to obtain an understanding of the self-organization of earthquakes. The Burridge–Knopoff (BK) model (Burridge & Knopoff 1967) models a fault by a spring-block system lying between two rigid tectonic plates; it reproduces the Gutenberg–Richter law. By including a relaxation time, Hainzl *et al.* (1999) also reproduced the Omori law and the increase with time of the foreshock frequency.

Our approach can be compared with renormalization techniques used for other examples of critical point phenomena in different areas of physics (Binney *et al.* 1992). It can be seen as a link between the physical approaches noted above, the BK multi-blocks approach and the scaling approaches to earthquakes. In previous work (Allègre *et al.* 1995, 1998) we modelled a fault zone with a hierarchical system made of embedded cells. Earthquakes that occur within the fault zone are the result of tectonic loading. Each earthquake is a critical phenomenon that is the expression of a self-organization of fractures at all scales. This view is supported by field observation (King 1983) and laboratory experiments (Tapponnier & Brace 1976). The potential elastic energy coming from the outside increases the density d of cracks at the lowest level; the density of cracks at higher levels is directly calculated from d by a criterion of coherent fracture organization (which we call the SOFT rule; Allègre *et al.* 1982). The cornerstone of this former SOFT approach (which we call the integral approach) is the appearance of a critical density of cracks d_c; the density of cracks versus d at a given level k tends toward a (Heaviside) step function $H(d-d_c)$ with increasing k. The whole organization process, through all scales, is completed during a chosen unit of time and, after an event, part of the energy is redistributed in the unbroken part of the medium, while another part is emitted by acoustic waves or consumed by friction. With this kind of approach it is possible to obtain some characteristic classes of seismic behaviour (seismic noise, swarms, earthquakes with or without precursors; Allègre *et al.* 1995) and a typical time distribution of aftershocks (Allègre *et al.* 1998), and also, following somewhat different lines, to generate an algorithm of prediction based on the variation of the local slope of the

magnitude–frequency relationship (Blanter *et al.* 1997). A large range of critical behaviours is also observed depending on the fracture criterion (Shnirman & Blanter 1999).

The present model is an implementation and an improvement of the integral approach; we now study a hierarchical system of identified cells, each of them being in one of a given number of states. Non-stationary transition rates between the various states and a stochastic process at the lowest scale define the location in time and space of each transition. We can determine the origin (in time and space) of the modelled structures (fractures) and their history on different time-scales. Our basic assumptions are as follows: the rupture can be initiated by the fracturing of a solid part of the medium (asperity) or can take place in a broken part through the friction process. The rupture can propagate until it is stopped by more solid parts (barriers; Aki 1984). These more solid parts of the medium favour in turn the loading up of the shear stress, which can be eliminated by both earthquakes and creep processes. We also include healing of cracks and a direct cascade (from higher levels to lower levels) of stress redistribution after each event. The stress redistribution generates small-scale stress heterogeneities from which one can compute the stress field at different scales. A time delay is precisely defined using the shear wave velocity, and this implies a more sophisticated SOFT rule with memory. We can describe the nucleation phase and the coseismic phase of an earthquake in terms of a cascade model (Ellsworth & Beroza 1995). A low frequency of the stick–slip behaviour at the smallest scale can be associated with the seismicity along creeping faults or during slow earthquakes. We eventually generate long-duration synthetic catalogues containing the time, magnitude and location of the events.

We will somewhat systematically compare the model results with seismicity observations. We are aware that confrontation of theory and experience cannot, in the present case, lead to what could be called a proof of the validity of our approach. We will come back to this point in Section 5.

2 THE GENERAL MODEL

In this paper we use the integral approach of the SOFT model (Allègre *et al.* 1995, 1998) as a starting point for a stochastic time-dependent model of a fault zone in which we incorporate the stress redistribution following seismic events. Indeed, in a homogeneous system the redistribution of stress at different scales and locations is the main cause of the heterogeneous distribution of cracks.

We propose first a general model that assumes the coexistence only of 'friction' along existing fractures and 'brittle fracture' of the solid parts of the medium ('asperities', 'barriers'). These two rupture mechanisms are then independently studied and their characteristic behaviour described, as well as the seismic phenomena they are associated with. The first variant, the 'friction' model, starts from a completely fractured state (all the cells, at all scales, are broken) and there is no healing process. In the second variant, the 'brittle fracture' model, we neglect friction and assume that only the solid (unfractured) part of the medium concentrates the elastic potential energy; rupture is initiated in a solid part and can propagate in the fractured part. The rupture threshold is constant for each model but larger in the case of the fracturing process.

Let us present our basic assumptions. The seismicity generation process takes place in a certain domain of a fault

zone. This domain is modelled by an abstract hierarchical system composed of embedded $\mathscr{D}$-dimensional cells in the manner explained in Fig. 1 (with $\mathscr{D}=2$): the highest level is associated with one cell and is subdivided into $\mathscr{R}^{\mathscr{D}}$ cells of the same shape, $\mathscr{R}$ being the renormalization factor. For each of these cells we repeat the same operation until we obtain a hierarchical stem of cells with $\mathscr{K}$ different scales. Let $k=0$ be the smallest scale, and $k=\mathscr{K}$ the largest. Our model is based on the simultaneous consideration of all scales. It is important to stress that our hierarchical system of cells does not represent a system of solid or quasi-solid blocks. Each cell at each level instead represents a boundary between two blocks, or a fracture. It can then be associated with a possible fault plane that is located somewhere within this cell. Each cell (crack) will interact with neighbouring cells (cracks) and possibly create a fracture at a larger scale in a larger cell.

We assume that, as a result of the long-term, large-scale, tectonic fracturing process, our system is polarized in the direction of the fault plane of the largest possible fracture. We shall call this direction the 'main direction'. For the sake of simplicity, we assume that the rupture propagates only along this 'main direction'. We only study the case of simple-shear stress loading, which corresponds to a strike-slip earthquake faulting mode. This idealized geometry can be modelled by a 2-D hierarchical system that represents a plane (Fig. 1, $\mathscr{D}=2$). The source of this loading is the motion of two tectonic plates in opposite directions. We assume a constant rate of motion and a constant normal stress; accordingly, shear stress would increase constantly but for the strain energy dissipated by earthquakes or non-elastic deformation (creep, plastic deformation). This process is associated with both discontinuous energy dissipation and temporal variation of the average shear stress. Furthermore, the complex geometry of fracturing creates a heterogeneous stress distribution. We neglect the heterogeneity of elastic and fragile properties of the medium.
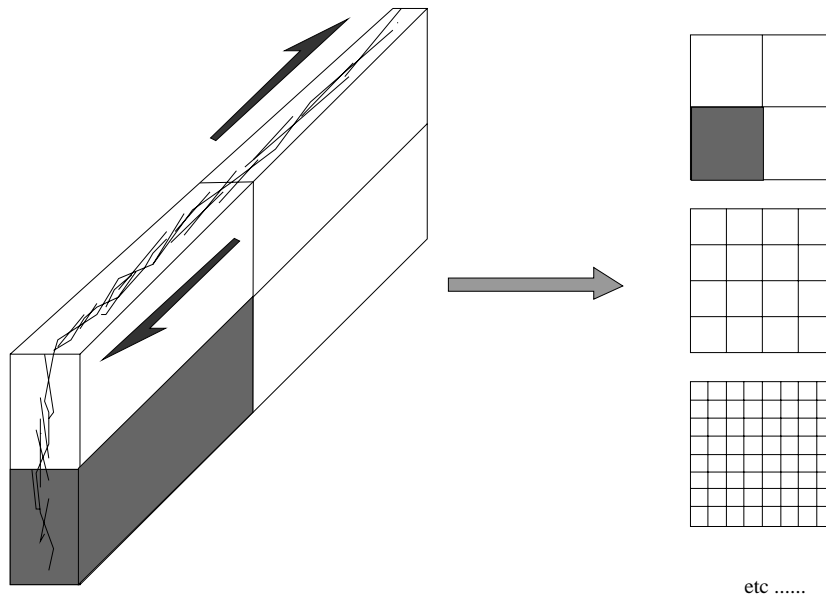
According to Båth, the duration of an earthquake, τ, defined as the rupture time, has the following empirical dependence on magnitude:

$$\log \tau = \log\left(\frac{\mathscr{L}}{v_{\mathrm{r}}}\right) = 0.5M + 1.9\,, \tag{1}$$

where $\mathscr{L}$ is the earthquake fault length, v_{r} the fracturing velocity and M the earthquake magnitude. A larger earthquake has a longer duration, and while part of the earthquake fault continues to move, some other parts have already stopped, and during the fracturing process it is impossible to determine the final magnitude of the event. In this paper we consider a constant rupture velocity of the order of the magnitude of the shear wave velocity.

We now discuss in more precise terms the stochastic dynamical system that we study in this paper.

2.1 The hierarchical system

The hierarchical system is obtained, as mentioned above, by dividing a $\mathscr{D}$-dimensional cell into $\mathscr{R}^{\mathscr{D}}$ smaller cells, $\mathscr{K}$ times. There are thus $n(k)=\mathscr{R}^{\mathscr{D}(\mathscr{K}-k)}$ cells at scale k, $k=0, \ldots, \mathscr{K}$. Let us denote by $C=C_i^k$, $i \in \{1, 2, \ldots, \mathscr{R}^{\mathscr{K}-k}\}^{\mathscr{D}}$ the $\mathscr{R}^{\mathscr{D}(\mathscr{K}-k)}$ cells of scale k and by $\Lambda_j(C_i^k)$, $j < k$, all the cells of scale j contained in C_i^k (Fig. 1). In the case where $j \geq k$, $\Lambda_j(C_i^k)$ stands for the unique cell of scale j in which C_i^k is included. Thus $\Lambda_k(\Lambda_{k+1}(C))$ are all the cells of level k contained in the same cell of the next larger-scale cell that contains C. At each moment any cell can be in three possible states:

  (1) solid (unfractured or unbroken): state s;
  (2) broken (locked by friction, fractured and motionless): state b;
  (3) moving (active): state m;

$C \in \{s, b, m\}\,.$

Figure 1. Abstract representation of a fault zone: opposing tectonic motions on either side of the fault zone generate an increase in microcrack density. We study the rupture phenomena on different scales through a hierarchical system. Here we draw the hierarchical system used with $\mathscr{D}=2$ and $\mathscr{R}=2$.

The characteristic length of a cell of scale k is

$$l(k) = l_0 \mathcal{R}^k , \tag{2}$$

where l_0 is the length of the cells of the elementary level. For a given cell of scale k, to be in the state solid means that there is no fracture of length $l(k)$ in it. On the other hand, a broken or a moving cell has fractures of size $l(k)$. A broken cell is weaker than a solid one, and consequently a smaller shear stress suffices to initiate its motion. A moving cell corresponds to a rupture of size $l(k)$ taking place. The propagation of this rupture is not instantaneous but rather takes a characteristic time, ΔT^k. Due to our assumption of a constant rupture velocity, this means

$$\Delta T^k = \frac{l(k)}{v_r} \tag{3}$$

(however, see Section 3.2). After defining the state transitions, we describe the smallest-scale dynamics, then the inverse cascade (from small scales to large scales) of rupture (fracture and friction) and finally the dynamics of the direct cascade (from large scales to the smallest scale) of stress redistribution.

2.2 The state transitions

There are four possible transitions for the cells (see Fig. 2):

$$s \rightarrow m , \tag{4}$$

$$b \rightarrow m , \tag{5}$$

$$m \rightarrow b , \tag{6}$$

$$b \rightarrow s . \tag{7}$$

Fracturing. The $s \rightarrow m$ transition is associated with a fracturing process. By this transition, we model the brittle behaviour of rocks under a given state of stress: the appearance of new cracks, crack development and cracking along old healed cracks. We do not detail any precise failure mechanism but consider only the initiation of cracks and their propagation along distance $l(k)$. This phenomenon implies motion of both sides of the crack.
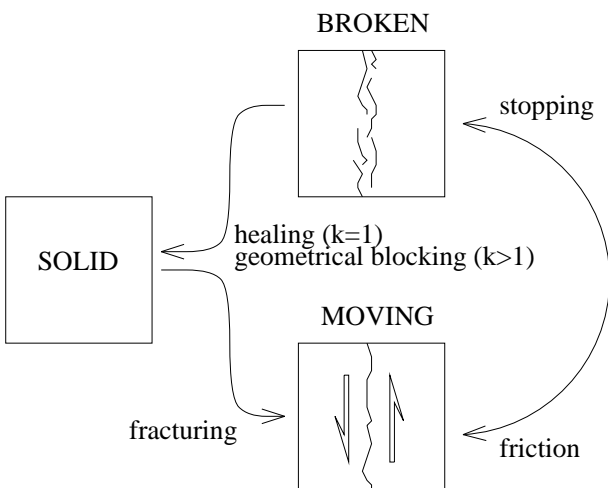
Figure 2. Different possible states of a cell and possible transitions. Note that the $s \rightarrow b$ and $m \rightarrow s$ transitions are forbidden.

$b \rightarrow m$ and $m \rightarrow b$ are the two transitions that constitute the stick–slip process.

Friction. The $b \rightarrow m$ transition is associated with a friction process. The slip takes place on an irregular fractured surface (microfault plane). During all the broken state time, the opening of the crack is kept constant; we neglect the complex geometry of this pre-existing crack.

Stopping. Corresponding to a stress drop, the $m \rightarrow b$ transition represents the stopping of both rupture processes (friction and brittle). The locally accumulated shear stress is released by the motion of the sides of the old or of the new crack. When the release is great enough, the motion stops and the sliding surface becomes a static microcrack (broken state).

Healing. The $b \rightarrow s$ transition is associated with a healing process. This phenomenon results from physico-chemical processes at the microscopic scale in rocks: compaction in the presence of fluid, grain growth and crack crystallization. We consider that a healed crack has the same mechanical properties as a part of the rock material that has never been fractured.

The two other transitions do not occur since a solid cell first starts moving and stays sliding during ΔT^0 before it becomes broken (recall that broken means fractured but not moving); moreover, a moving cell can obviously not become solid without stopping.

2.3 The smallest scale

We define the whole process in terms of non-stationary transition rates between the various states. In general, these transition rates will depend on the present state of a cell and on its past, as well as on the past of its neighbouring cells. At the smallest scale it depends in addition on the local stress, which changes as a result of seismic events and global large-scale loading.

We attach to each cell $C = C^0$ a real number, $\sigma = \sigma(C, t)$, that varies with time and represents the local accumulated stress. The dynamics at the smallest scale are given by a time-dependent stochastic process. In the following we write $\alpha_{u \rightarrow v}$ for the variable transition rate from state $u \in \{s, m, b\}$ to $v \in \{s, m, b\}$. Recall what this means that given that a cell is in state u, the probability that it undergoes a transition towards the state v in the infinitesimal time interval dt is $\alpha_{u \rightarrow v} dt$. The transition rate for $b \rightarrow s$ is fixed to some constant value β, which is independent of the state of the system:

$$\alpha_{b \rightarrow s} = \beta . \tag{8}$$

We neglect the complex dependence on physical parameters such as temperature, local pressure and amount of fluid of the geochemical healing process ($b \rightarrow s$).

The transition rate $s \rightarrow m$ depends on the local stress only. For its dependence on the local shear stress we use the following expression ($\sigma = \sigma(C, t)$):

$$\alpha_{s \rightarrow m}(\sigma) = \begin{cases} 0 & \text{for } \sigma \leq \sigma_s , \\ k_s \left(\dfrac{\sigma - \sigma_s}{\sigma_s} \right)^{\delta_s} & \text{for } \sigma > \sigma_s , \end{cases} \tag{9}$$

where σ_s is the fracture threshold, k_s is a constant with dimensions of the inverse of time and δ_s is some phenomenological material constant.

The transition rate $m \to b$ is deterministic:

$$\alpha_{m \to b}(t) = \delta(t - [t_0 + \Delta T^0]). \tag{10}$$

Here $t_0 = t_0(t)$ is the time when the cell became moving for the last time and ΔT^0 is a time delay (see eq. 3). In other words, a cell that has started to move becomes broken (and not moving) after a time ΔT^0. A constant rate of stress release (stress drop) during ΔT^0 justifies this assumption.

The transition rate $b \to m$ has two contributions corresponding to two different possible mechanisms:

$$\alpha_{b \to m} = \alpha_{b \to m}^1 + \alpha_{b \to m}^2. \tag{11}$$

The first is the analogue of the transition $s \to m$. It is a spontaneous random transition that depends only on the actual local stress in the cell:

$$\alpha_{b \to m}^1(\sigma) = \begin{cases} 0 & \text{for } \sigma \leq \sigma_b, \\ k_b \left(\dfrac{\sigma - \sigma_b}{\sigma_b} \right)^{\delta_b} & \text{for } \sigma > \sigma_b, \end{cases} \tag{12}$$

where σ_b is the friction threshold, k_b is a constant with dimensions of the inverse of time and δ_b is some phenomenological material constant.

The second contribution corresponds to a transition that is induced by some neighbouring cell (intrascale propagation): a broken cell starts moving at time ΔT^0 (intrascale growth of 'fracturing') after a neighbouring solid cell along the main direction starts moving (nucleation of the 'fracturing'). In more precise terms, a broken cell becomes moving at time t if at time $t - \Delta T^0$ one of its 'neighbours' underwent a transition from solid to moving. Here the 'neighbouring' cells of C are those in the set $\Lambda_0(\Lambda_1(C))$ (the $\mathscr{R}^{\mathscr{D}}$ cells within the same cell of scale 1 that contains C) that lie along the main direction with respect to C. Thus

$$\alpha_{b \to m}^2(t) = \delta(t - [t_0 + \Delta T^0]), \tag{13}$$

where $t_0 = t_0(t)$ is now the latest time point when a neighbouring cell (in the above sense) underwent a transition $s \to m$. Such an *intrascale propagation* will also hold for scales $k > 0$ (see below). The intrascale propagation direction is the same as the direction involved in the critical rule of the interscale rupture propagation (SOFT rule), which we detail in the next section.

In our numerical experiment we will denote by $\pi(t)$ the sum of all the transition rates, at time t, at the elementary level of the hierarchical system. It is a measure of the actual stochastic activity in our system.

2.4 The inverse cascade of 'fracturing', 'friction' and 'blocking'

In previous papers on the SOFT model (Allègre *et al.* 1995, 1998), only solid and broken cells were considered in the hierarchical system. The transfer of fracturing from lower levels to upper levels (inverse cascade) was determined by a simple rule: if at least one straight line (following the main direction) of cells ($\mathscr{R}$ cells) of level k is composed only of broken cells, the corresponding cell of level $k + 1$ is also broken (Fig. 3). In this case the state of all cells at all levels is entirely determined by the configuration at the smallest scale. At each time, the state of larger scales is a function of the instantaneous
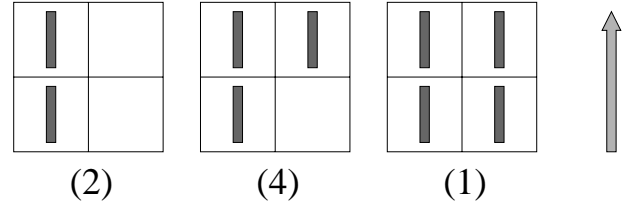
Figure 3. The critical configurations of the SOFT rule ($\mathscr{D} = 2$, $\mathscr{R} = 2$). The number of critical configurations for a given number of broken or moving cells is given in brackets. The arrow indicates the 'main direction'.

picture at the smallest scale. The different scales do not have any proper dynamics since they are, so to speak, 'slaves' of the smallest scale.

Here we consider a system with a memory, a next-neighbour correlation (*cf*. the intrascale propagation) and a more elaborate SOFT rule. The new SOFT rule associates with a cell C at level k a 'virtual' state that is a function of the configuration of the $\mathscr{R}^{\mathscr{D}}$ cells in $\Lambda_{k-1}(C)$. However, the 'real' state of C will also depend on its history and on its next neighbours. No additional stochasticity is introduced at scales larger than the elementary scale ($k = 0$).

The new SOFT rule is as follows: $C = C_i^k$ is 'virtually' moving if the moving cells in $\Lambda_{k-1}(C)$ are in a critical state with respect to the classical SOFT rule. C is 'virtually' broken if the broken cells in $\Lambda_{k-1}(C)$ are in a critical state with respect to the classical SOFT rule. In the case of a conflict between the two rules, the moving rule prevails. In all other cases C is 'virtually' solid.

The rules for the various transitions of a cell of level k are as follows.

(1) Suppose C is in the solid state. It undergoes the transition solid $\to$ moving if it becomes 'virtually' moving.

(2) Suppose C is in the moving state. It undergoes the transition moving $\to$ broken at time t if it started to move at time $t - \Delta T^k$. That means that, once it starts moving, it stays moving for ΔT^k (according to eq. 1) before it becomes broken. Therefore, it may happen that, while a cell is moving, the smaller-scale configuration changes in such a way that it becomes 'virtually' non-moving; nevertheless, the cell keeps moving until the time ΔT^k is completed. This is the main difference between our new concept with memory and the classical static SOFT rule: if, as in Allègre *et al.* (1995), the moving state at all scales $k \neq 0$ is a function of the instantaneous configuration at scale $k = 0$, the lifetime of the moving cells (the average duration of the moving state during the numerical experiment) can be smaller for higher degrees. We show this difference with the simplest example: $\mathscr{R} = 2$, $\mathscr{K} = 1$, $\mathscr{D} = 1$. The hierarchical system is made of two cells C_1^0 and C_2^0 of level 0, aligned along the main direction and included in the unique cell C_1^1 of level 1. If the cell C_1^0 starts to move at t_1 for an interval of time ΔT^0, and the cell C_2^0 starts to move at $t_2 \in [t_1; t_1 + \Delta T^0]$ for an interval of time ΔT^0, C_1^1 is moving: (a) during $[t_2; t_1 + \Delta T^0]$ in the case of the static SOFT rule; (b) during $[t_1; t_1 + \Delta T^1]$ in the present case of the SOFT rule with memory.

(3) Suppose C is in the broken state. It undergoes the transition broken $\to$ solid if it becomes 'virtually' solid (hierarchical geometric blocking). We extract from the simplest example (as above $\mathscr{R} = 2$, $\mathscr{K} = 1$, $\mathscr{D} = 1$) some interesting behaviour: if C_1^0 is broken during $[t_1; t_1 + \Delta t_1^\beta]$ and C_2^0 is broken

during $[t_2; t_2 + \Delta t_2^\beta]$ with $t_2 \in [t_1; t_1 + \Delta t_1^\beta]$, C_1^1 is only broken during $[t_2; \min(t_1 + \Delta t_1^\beta, t_2 + \Delta t_2^\beta)] \leq (\Delta t_1^\beta + \Delta t_2^\beta)/2$ (superscript β indicates that Δt intervals are related to the broken state lifetime). Consequently, even if physico-chemical healing processes are longer the larger the scale is, the process of healing by geometrical blocking (non-cooperative behaviour at smaller scales) can be more rapid for larger fractures. This is due to the increase of possible blockings ('barriers') at every smaller scale.

(4) Suppose C is in the broken state. It undergoes, at time t, the transition broken $\rightarrow$ moving if it becomes 'virtually' moving at time t, or, if at time $t - \Delta T^k$, one of its solid neighbours in $\Lambda_k(\Lambda_{k+1}(C))$ lying in the main direction with respect to C started moving (intrascale propagation, already mentioned in Section 2.3 for the 0 scale).

Bear in mind that the inverse cascade of rupture is instantaneous according to the SOFT rule. Consequently, a transition at the lowest level could correspond to a similar transition at higher levels. This does not mean that the rupture process itself is instantaneous because this process is in fact made of all the ruptures at lower levels that occurred before this transition (intrascale propagation and SOFT rule with memory).

2.5 The direct cascade of stress redistribution

We detail here the source of the stress heterogeneity. As we saw in the previous section, the small-scale dynamics depends on the local stress in elementary cells C_i^0, $i \in \{1, 2, \ldots, \mathscr{R}^{\mathscr{K}-k}\}^{\mathscr{D}}$. This local stress is changed on the one hand by the external large-scale loading process, and on the other hand by the internal stress redistribution following the seismic events (varying with time),

$$\frac{d\sigma(C_i^0, t)}{dt} = E + I_i(t), \tag{14}$$

where E (assumed to be constant) and $I_i(t)$ are respectively the external loading rate and the internal stress redistribution rate. A seismic event is a cell in the moving state (see, however, Section 3.2). For a cell C_j^k of level k we denote by $T^s(C_j^k)$ and $T^b(C_j^k)$ the sets of time points τ^s and τ^b when it starts to move from a solid and a broken state, respectively. For the sake of simplicity we assume that the stress is redistributed uniformly in time during the event. Therefore, we write $I_i(t)$ as follows:

$$I_i(t) = I_i^s(t) + I_i^b(t), \tag{15}$$

$$I_i^s(t) = \sum_{k=0}^{K} \sum_{C_j^k} \sum_{\tau \in T^s(C_j^k)} \xi_{[\tau, \tau + \Delta T^k]}(t) \frac{\Delta^s \sigma_{i,j}^k}{\Delta T^k}, \tag{16}$$

$$I_i^b(t) = \sum_{k=0}^{K} \sum_{C_j^k} \sum_{\tau \in T^b(C_j^k)} \xi_{[\tau, \tau + \Delta T^k]}(t) \frac{\Delta^b \sigma_{i,j}^k}{\Delta T^k}, \tag{17}$$

with

$$\xi_{[\tau, \tau + \Delta T^k]}(t) = \begin{cases} 1 & t \in [\tau, \tau + \Delta T^k] \\ 0 & \text{otherwise} \end{cases}.$$

Thus $\Delta^s \sigma_{i,j}^k$ and $\Delta^b \sigma_{i,j}^k$ are the amounts of stress, during time ΔT^k, internally redistributed into the cell C_i^0 of the elementary level when a cell C_j^k has moved from a solid or a broken state. For each transition through the moving state, three contributions are taken into account. Suppressing the indices s and b,

we have

$$\Delta \sigma_{i,j}^k = \Delta \sigma_{\text{loc};i,j}^k + \Delta \sigma_{\text{red};i,j}^k + \Delta \sigma_{\text{unif};i,j}^k, \tag{18}$$

where $\Delta \sigma_{\text{loc}}$, $\Delta \sigma_{\text{red}}$, $\Delta \sigma_{\text{unif}}$ are respectively the local stress drop, the redistribution of stress from neighbouring cells, and the uniform stress drop.

First, if a cell $C = C_j^0$ at the elementary level moves, it undergoes a local stress drop that we assume to be constant. This local stress drop does not happen for moving cells at higher levels and thus

$$\Delta \sigma_{\text{loc};i,j}^k = -\sigma_{\text{loc}} \delta_{ij} \delta_{k0}. \tag{19}$$

Second, if cells at higher level move, they induce a stress redistribution in adjacent cells. To model this stress redistribution we introduce for each scale k a mask F_l^k, $l \in \{-1, 0, +1\}^{\mathscr{D}}$, that, for each event, determines the change of local stress in the neighbourhood of the cell where the event took place. For simplicity we only consider the next and next-nearest neighbours. Moreover, we assume that all the redistribution masks are obtained via a scaling of the mask at the smallest scale F^0. More precisely, if an event takes place in a cell C_j^k of level k, the stress in the elementary cell C_i^0 changes according to the following formula:

$$\Delta \sigma_{\text{red};i,j}^k = \begin{cases} F_l^k, & \text{if } C_i^0 \in \Lambda_0(C_{j+l}^k), \ l \in \{-1, 0, +1\}^{\mathscr{D}} \\ 0 & \text{otherwise} \end{cases}. \tag{20}$$

The mask F_l^k is derived from F_l^0 according to the rule

$$F_l^k = \lambda \mathscr{R}^{\theta k} F_l^0 \tag{21}$$

with some parameters θ and λ. The boundary is treated by 0-extension.

For a typical example in two dimensions, see Fig. 4, where we approximate in a discrete and abstract way the actual observed redistribution patterns (Okada 1985, 1992). Four parameters are used to define the mask F^0 in two dimensions. Here, we simply consider that there is a relative increase of the shear stress along the main direction (A_0, A_1 on Fig. 4) coupled with a relative decrease in the other direction (A_2 in Fig. 4); these relative variations represent a few per cent of the local shear stress. Note that, with these definitions, an event of scale k affects the stress in all the smallest-scale cells located in the neighbourhood of C_j^k (direct cascade); this neighbourhood grows proportionally to $l(k)$. As mentioned in Section 2.4, an event at the elementary scale may instantaneously produce larger-scale events through the inverse cascade; the stress
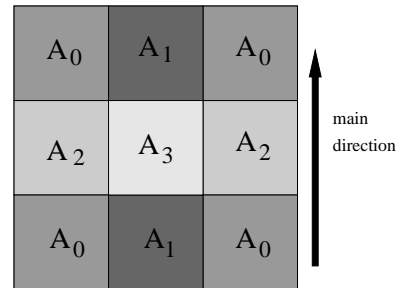

Figure 4. Typical stress redistribution pattern generated by the motion of the central cell (subject itself to a stress change A_3) (for any level k). The shear stress increases along the main direction ($A_1 > A_0 > 0$) and decreases along the other direction ($A_2 < 0$).

redistribution corresponding to these events generates a large heterogeneity in the stress field through the direct cascade. This is one of the key points of the model: multiscale interactions govern the seismogenic process.

Third, an event at scale k is assumed to produce a total global stress drop $\Delta\sigma_{\text{glob}}^k$, which we will specify below. In order to respect this constraint, we add, in the case of an event at scale k, to every cell of the elementary level a uniform stress change,

$$\Delta\sigma_{\text{unif};i,j}^k = \Delta\sigma_{\text{unif}}^k, \quad \text{such that} \quad \sum_i \Delta\sigma_{i,j}^k = \Delta\sigma_{\text{glob}}^k, \quad \forall j. \quad (22)$$

Let us show in detail how we calculate the global stress drop, $\Delta\sigma_{\text{glob}}$. Kostrov (1974) has suggested a formula generalizing Brune's (1968) formula to the case of a seismic process taking place in a volume V. Each event of seismic moment M_0 is associated with a negative variation of the average strain, $\Delta\varepsilon_{\text{a}}$,

$$\Delta\varepsilon_{\text{a}} = -\frac{M_0}{2\mu V}, \quad (23)$$

where μ is the shear modulus. The corresponding change of the average stress, $\Delta\sigma_{\text{a}}$, is

$$\Delta\sigma_{\text{a}} = \mu\Delta\varepsilon_{\text{a}} = -\frac{M_0}{2V}. \quad (24)$$

In our hierarchical system, the seismic moment, $M_0(k)$, of an event of level k is given by

$$M_0(k) = \mu S(k)u(k), \quad (25)$$

where $u(k)$ is the displacement caused by the event and $S(k)$ is the fault surface area. The displacement is proportional to the linear size of the corresponding moving cell ($u(k) \sim \mathscr{R}^k$), while the surface is the product of the length $l(k)$ of the cell and its height $h(k) \sim l(k)$: $S(k) \sim \mathscr{R}^{2k}$. It follows that

$$M_0(k) = \mu_1 \mathscr{R}^{3(k-\mathscr{K})}, \quad (26)$$

where $\mu_1 \sim \mu l^2(\mathscr{K})u(\mathscr{K})$ is a constant. From eqs (24)–(26), the global stress drop, $\Delta\sigma_{\text{glob}}$, due to an event of level k, is

$$\Delta\sigma_{\text{glob}}(k) = -\mu_2 \mathscr{R}^{3(k-\mathscr{K})}, \quad (27)$$

where $\mu_2 \sim 0.5\mu l^{-1}(\mathscr{K})u(\mathscr{K})$ (we assume $V \sim l^3(\mathscr{K})$). From eqs (18) and (22), we deduce the uniform stress drop, which is redistributed in the whole domain.

3   A 'FRICTION' MODEL AND A 'FRACTURING' MODEL

The general model described above has very complex behaviour, and no large range of parameters values has yet been explored. Therefore, in the present paper we examine two submodels that have been explored in some detail and constitute the first two steps of a complete numerical simulation that will be explored in a future study. Considering the two submodels separately is a preliminary approach to understanding the origin of the different characteristics of the general model. We study here two distinct ranges of parameters, one that corresponds to a 'fracturing' model and the other that corresponds to a 'friction' model. They do not describe the faulting mechanism at the same timescale; they are in fact complementary submodels of the more complete model that corresponds to the theoretical formalism examined above (Section 2). For the sake of simplicity

and to save on computation time, we consider in the following $\mathscr{D} = 2$. If we conserve our anisotropic SOFT rule (the critical configuration is an alignment along only one particular direction) and our schematic stress redistribution mechanism, which again introduces anisotropy, a 3-D approach would not constitute a major change in principle (see Section 2, Figs 3 and 4), even if, in the classical renormalization techniques, the dimensionality of the system exerts an important control on its behaviour. Nevertheless, a full realistic 3-D approach would not be so simple to implement, given that faults may occur in different orientations, and that the addition of gravitational effects may be significant.

3.1   A 'friction' model

This model corresponds to a completely fractured fault zone. To study this 'friction' process starting from our general model, we simply take a completely broken initial state (all the cells, $\forall k$, are broken) without healing process ($\beta = 0$) (see Table 1c).

We give the basic properties of this simpler model within the framework of the general model. We are left with two states, broken and moving. The transition $b \rightarrow m$ at the elementary level is determined by a stochastic random process (eq. 12), whilst at higher scales ($k > 0$) it is determined by the SOFT rule

Table 1. (a) Parameters that are kept constant in both models ($\Delta\sigma_{\text{loc}} = \Delta\sigma_{\text{loc}}^s = \Delta\sigma_{\text{loc}}^b$); (b) parameters of the 'fracturing' model; (c) parameters of the 'friction' model.

(a)	
$\mathscr{R}$	2
$\mathscr{D}$	2
v_{r}	3000 m s^{-1}
σ_b	100 bar
σ_s	110 bar
$\Delta\sigma_{\text{loc}}$	30 bar
μ_2	$2\,\mathscr{R}^{\mathscr{D}\mathscr{K}}$ bar
E	10^{-9} bar s^{-1}
k_s	10^{-4} s^{-1}
δ_s	3
δ_b	1.5

(b)	
	'Fracturing' model
$\mathscr{K}$	6
β	3×10^{-11} s^{-1}
k_b	$\rightarrow \infty$
θ^s	1.5
$A_{i=\{0,\dots,3\}}^s$	$1, 2, -7, 0$
λ^s	5.8×10^{-2} bar
initial condition	completely solid
event	$s \rightarrow b$

(c)	
	'Friction' model
$\mathscr{K}$	4
β	0
k_b	2.5×10^{-2} s^{-1}
θ^b	0.5
$A_{i=\{0,\dots,3\}}^b$	$1, 2, -4, -8$
λ^b	2 bar
initial condition	completely broken
event	m

applied to the cells of the lower level $(k-1)$. The transition $m \to b$ is deterministic at all scales k; a cell stops moving a time ΔT^k after it started moving at time t. If during this time span $(t, t+\Delta T^k)$, the moving cell becomes virtually moving again (because at smaller scale a SOFT configuration occurs) it will still stop at $t+\Delta T^k$.

Before generating a seismic catalogue (time, magnitude, location), let us define what we call in this model an earthquake, its magnitude and its nucleation time and location. We define the nucleation time point and its position in a recursive way. If a cell C at level k starts moving, it either participates in the nucleation of an event of larger scale $k+1$, or it represents the endpoint of a 'friction' cascade. It is the endpoint in a 'friction' cascade, if, during its moving time ΔT^k, the cell $\Lambda_{k+1}(C)$ does not start moving. Note that $\Lambda_{k+1}(C)$ may already be moving, in which case the event occurring at C is automatically the endpoint of a friction cascade. We say that a cell C of level k participates in the nucleation of an event if during ΔT^k, its moving time, the cell $\Lambda_{k+1}(C)$ undergoes a transition to the moving state as well. This motion, however, may have been initiated by some other cell in $\Lambda_k(\Lambda_{k+1}(C))$. We now define the nucleation location and time at scale k of a larger event of scale $k+1$: it is the position of the first cell in $\Lambda_k(\Lambda_{k+1}(C))$, lying in the main direction with respect to C, that started to move and the time when it started to move. This defines in a recursive way the nucleation location and time of any event at the smallest scale. In the case where a cell C^k at level k is the endpoint of a cascade (see above), we report in the catalogue its nucleation time and location at the elementary scale through the recursive scheme described above; we say that an earthquake of level k was initiated at this time point and location.

An earthquake of level k is associated with the moving state of a cell of level k. This event has to be given a magnitude completely defined by its level k. This magnitude, $M(k)$, can be obtained from eq. (26) using the relationship $\log(M_0(k)) = 1.5M(k) + \text{const}$, or directly from $M(k) = \log(S(k)) + \text{const}$ (Kanamori & Anderson 1975). In both cases, we obtain

$$M(k) = 2k \log(\mathscr{R}) + \text{const}. \tag{28}$$

Let us state some characteristics of the model. First, we can describe the nucleation phase, the coseismic phase and the stopping phase of an earthquake (see Section 4.3) as a cascade model (Ellsworth & Beroza 1995). Second, the propagation of the moving state (due to stress redistribution) at the elementary level can proceed at different rates and may or may not be associated with a higher-scale event. We illustrate different situations in the 1-D case of Fig. 5 (N and t_i are defined in the caption).

(1) $t_N - t_1 \gg \Delta T^{\mathscr{K}}$: the propagation proceeds very slowly and there is no highest-level event; this corresponds to the seismicity along creeping faults (we call this behaviour creep).
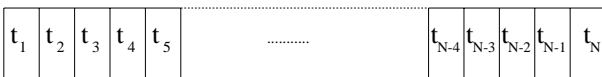
(2) $t_N - t_1 > \Delta T^{\mathscr{K}}$: the propagation proceeds slower than the rupture and there is no highest-level event; this corresponds to the seismicity during a slow earthquake.

(3) $t_N - t_1 \leq \Delta T^{\mathscr{K}}$: the propagation is very rapid and there is an event of the highest scale with a stick-slip mechanism.

3.2 A 'fracturing' model

As in our previous approach (Allègre *et al.* 1995, 1998), this model corresponds to a weakly fractured fault zone where the healing process is effective at the lowest scale ($\beta \neq 0$). This process generates a hierarchical geometric blocking at higher scales. To distinguish the 'fracturing' submodel from the general model, we simply adopt (see Table 1b) an instantaneous propagation of rupture ($\Delta T^k \to 0, \forall k$) and a continuous shear stress dissipation by friction. Thus we end up with a two-state model, solid and moving-broken. To incorporate the dissipation by friction, we let k_b go to infinity in eq. (12), in such a way that, as soon as the stress reaches the critical threshold value σ_b, the cell undergoes a transition $b \to m$ and stays moving for an infinitesimally small time ΔT^k before it becomes broken again. Note that the transitions $b \to m \to b$ are not visible in our condensed two-state (solid and moving-broken) 'fracturing' model. During the infinitesimal time ΔT^k, the excess of stress with respect to σ_b is eliminated from the system by the 'friction' process.

Let us recall, in the framework of the general model, the basic characteristics of this simpler model. We have two states, solid and moving-broken (we now use the term 'broken' for this double state). The transition $s \to b$ at the elementary level is determined by a stochastic random process (eqs 4–9), whilst at higher scales it is determined by the SOFT rule applied to the broken cells of the lower level. The transition $b \to s$ is also determined by the SOFT rule: a cell which is not in the broken state is in the solid one.

To generate a seismic catalogue (time, magnitude, location), let us define precisely what we call, in this model, an earthquake, its magnitude and its nucleation time and location. An earthquake is here associated with the $s \to b$ transition. Since the rupture instantaneously propagates through the higher levels, transition $s \to b$ at the elementary scale is called a 'hypocentre', which is the nucleation of the fracture, which can propagate through the scales, thanks to an inverse cascade. All these nucleations are noted in the catalogue. Of course, there is no earthquake duration in this case. For a given event, the magnitude is given by eq. (28), as in the 'friction' model.

4 RESULTS OF NUMERICAL SIMULATIONS

As mentioned above, we study two distinct ranges of parameters, one that corresponds to a 'friction' model and the other that corresponds to a 'fracturing' model. We are interested in the most general properties of the event sequences obtained from the numerical simulations; these are the magnitude–frequency relationship, the temporal variation of the number of foreshocks and aftershocks per unit of time and the periodicity of strong events. For both models, for a wide range of parameter values, event (earthquake) sequences perfectly obey both the Gutenberg–Richter law and the modified Omori law.

| t_1 | t_2 | t_3 | t_4 | t_5 | .... | t_{N-4} | t_{N-3} | t_{N-2} | t_{N-1} | t_N |

Figure 5. Ideal propagation of the friction (from left to right) in a 1-D hierarchical system ($N = \mathscr{R}^{\mathscr{K}}$). The t_i are the fracturing times of cells C_i and $t_i < t_j$ if $i < j$. Depending on the value of $(t_N - t_1)$, one obtains different kinds of seismic events (see text).

Let us discuss the parameters kept constant in each model (see Table 1a). $\mathscr{R}$ is taken equal to 2; a larger renormalization factor would only provide a more realistic magnitude–k relationship (eq. 28) and an increase in the number of fore-shocks and aftershocks (Allègre *et al.* 1998). The latter statement is still valid when considering the effect of an increase in the number of scales, $\mathscr{K}$ (see Fig. 12). A small number of scales is not a big drawback because of the self-similar behaviour at all scales except the elementary scale ($\mathscr{K}=0$); note that the typical length of an elementary cell is related to this number of scales. All the parameters concerning the stress field (σ_b, σ_s, $\Delta\sigma_{\text{loc}}$, μ_2) are of the order of the magnitudes of the observed ones. Parameters related to eqs (9) and (12) (δ_s, δ_b, k_s, k_b) are arbitrarily chosen.

4.1   Method of analysis

We obtain numerical catalogues of events (see above). These catalogues contain the times of events, the 'hypocentre' coordinates, the hierarchical level reached by the event and the corresponding magnitude (see eq. 28). We also follow the evolution of the total transition rate at the lowest scale, of the average shear stress, and of the heterogeneity of the stress field.

Making use of eq. (28) for the conversion from hierarchical level to magnitude, we estimate the b-value of the Gutenberg–Richter relationship through the formula

$$b = \frac{1}{2\log(\mathscr{R})}\log\left(1+\frac{1}{\overline{k}-k_{\text{m}}}\right), \tag{29}$$

where $\overline{k}$ and k_{m} are respectively the average and the minimum hierarchical levels in the set or subset of events considered. This formula is the maximum likelihood estimate of the b-value in the case of an unlimited range of discrete magnitudes with integer values (Molchan *et al.* 1997; Kulldorf 1961). The limitation of the magnitude of events by the highest scale in our model is not important for the comparative analysis. The magnitude band of the model is derived from the number of hierarchical levels through eq. (28), and the maximum magnitude is fixed by the characteristic length of the highest level.

For the temporal analysis of foreshocks and aftershocks, we used the program AFT developed by Utsu *et al.* (1995). This program is available in the IASPEI Program Library (Lee 1997). We estimated the parameters of two different models of after-shock decay (or foreshock increase): the modified Omori law (Utsu *et al.* 1995) and its modification, known as the Otsuka model (Otsuka 1985). The modified Omori model assumes a power-law decay:

$$f(t) = \frac{A}{(t+c)^p}, \tag{30}$$

where $f(t)$ is the number of events per time unit, t is the time since the main shock, p is the Omori exponent and c is a shifting parameter. In the Otsuka model the long tail of the power law is reduced by introducing an exponential with a characteristic time T:

$$f(t) = \frac{A}{(t+c)^p}\exp\left(-\frac{t}{T}\right). \tag{31}$$

The parameters of eqs (30) and (31) are computed with the program AFT using the maximum likelihood method and

the Davidson–Fletcher–Powel optimization procedure (Utsu *et al.* 1995). Unfortunately, this program does not work with sequences containing more than 5000 events. We developed our own code, which can be applied to unlimited sequences.

4.2   Identification of the events

Let ΔT_{aft} be a time span that will be defined below. Main shocks and aftershocks are identified in the following way:

if an event of level k at time t is preceded by only lower-level events in $[t-\Delta T_{\text{aft}}, t]$, it is a main shock with precursors;

if an event of level k at time t is not preceded by an event during $[t-\Delta T_{\text{aft}}, t]$, it is a main shock without precursors;

if an event of level k at time t is preceded in $[t-\Delta T_{\text{aft}}, t]$ by an event of level k that is not an aftershock, it belongs to a swarm of level k;

if an event of level k at time t is preceded by a higher-level event during $[t-\Delta T_{\text{aft}}, t]$, it is an aftershock.

ΔT_{aft} is chosen (by trial and error) in such a way that about 90 per cent of the aftershocks of a main shock (identified as described above) that occurred at time t are contained in $[t; t+\Delta T_{\text{aft}}]$. ΔT_{aft} depends essentially on the parameters of the mask. These rules are somewhat arbitrary, but we have observed that the results do not depend much on ΔT_{aft} if this value is a few orders of magnitude less than the average time interval between two main shocks.

4.3   Numerical results of the 'friction' model

In the 'friction model' $\pi(t)$ is the total transition rate $b\rightarrow m$ at the elementary scale and we will interpret in terms of foreshocks-main shock-aftershocks the short time period from the nucleation phase to the stopping phase of a given event.

'Friction' model with weak load. We assume a very small loading rate that will not change the system significantly during the characteristic duration of a foreshocks–main shock–aftershocks sequence. Starting from a homogeneous state, the system may have been loaded up to the critical stress value ($\mathscr{R}^{\mathscr{D}\mathscr{K}}\sigma_b$ bar) by the stress (E) applied to the boundary of the domain by plate tectonics. According to eq. (12), this is indeed possible in the case of a homogeneous system, because nothing occurs as long as $\sigma_i < \sigma_b$. We can take as the initial ($t=0$) configuration $\sigma_i = \sigma_a = \sigma_b \; \forall i$. A first transition $b\rightarrow m$ is randomly chosen in the volume. This first nucleation is enough to obtain, without additional loading, an increase in the fore-shock activity, a main shock and aftershocks. We explain this behaviour as follows. The perturbation of the stress field around the first moving cell ($\Delta\sigma_{\text{red}}$) is larger than the uniform stress change ($\Delta\sigma_{\text{unif}}$) calculated from the global stress change ($\Delta\sigma_{\text{glob}}$). Consequently, at the elementary level the rate of transitions $b\rightarrow m$ ($\pi(t)$) increases; the heterogeneity of the stress field increases after each event at the elementary level, and so on. The process is autoaccelerated, events at higher levels occur and, finally, a strong event may occur. This is the time of the largest stress field heterogeneity. A strong event (or strong events) significantly unloads the whole system. This starts the cascading of the aftershocks, which unloads the areas of high stress and decreases the average stress (σ_a). The value of $\pi(t)$ decreases rapidly at the beginning, but this decrease then slows down due to the decrease of σ_a.

The general results are as follows. First, in a very large range of model parameter values, we obtain sequences with an increasing frequency of foreshocks preceding a main shock or several strong events (swarm) followed by a sequence of aftershocks with decreasing density. Second, the temporal decay of the number of aftershocks per time unit obeys in general the modified Omori law, in many cases perfectly. The value of the power exponent is usually around 1.5. Third, the event size distribution follows the Gutenberg–Richter law very closely; *b*-values vary in the range 0.5–5.0, depending upon the different parameter value sets, and they also vary with time, for given parameters, during the foreshocks–main shock–aftershocks sequence. Fourth, foreshocks also often follow a power-law increase.

We now present in more detail the behaviour of the system for different values of the parameters equal to and close to those reported in Tables 1(a) and (c). Results corresponding to the parameter value sets of Tables 1(a) and (c) (the reference sequence) are shown in Fig. 6 against both linear (Fig. 6a) and logarithmic (Fig. 6b) timescales, calculated from the time of the first nucleation (see above). In both parts of the figure, the first graph shows the level of the events, the second shows the total transition rate $b \rightarrow m$ at the elementary scale, the third represents the evolution of the average global stress, the one the evolution of the standard deviation of the stress distribution for levels 0 and 1, and the last graph shows the density d of currently moving cells at the elementary level; note that at the moment of the main shock this number is less than at the time of the strong foreshocks. Both values of d are much less

than the critical density value (0.618) of the corresponding integral SOFT model. This 'reference' sequence summarizes the typical behaviour of the 'friction' model. The main shock is preceded by a short sequence of foreshocks. With the logarithmic timescale we clearly see the temporal clustering of events: strong foreshocks are themselves preceded by fore-shocks and have their own aftershocks. The main shock has a rather long sequence of aftershocks. Fig. 7 shows that the temporal aftershock activity decay with time obeys very well the modified Omori law. Fig. 7(a) shows on a logarithmic timescale the cumulative number of aftershocks compared with the theoretical curve (eq. 30) for the values $p = 1.52$, $c = 203$ given by the maximum likelihood estimation. Fig. 7(b) shows the cumulative number of aftershocks versus the number given by eq. (30).

The event size statistics follow the Gutenberg–Richter law. Fig. 8 shows separately the magnitude–frequency curves for foreshocks and aftershocks with *b*-values respectively equal to 1.43 and 2.06. The slope break for the magnitude–frequency curve for all events ($b = 1.85$) at $k = \mathcal{K} - 1$ is a finite size effect (only one highest-scale event is recorded in the analysed sequence). Fig. 9 shows the temporal variation of the *b*-value, estimated at time t by eq. (29) using the last 200 events before t. We see that the *b*-value has a minimum just before the main shock, as is often observed for large earthquakes (Smith 1981), even if not systematically. Such an observation was discussed in Main *et al.* (1990) and has been observed in controlled tests by Sammonds *et al.* (1992). These authors invoke a (short or prolonged) strain-softening mechanism. Similarly, in our
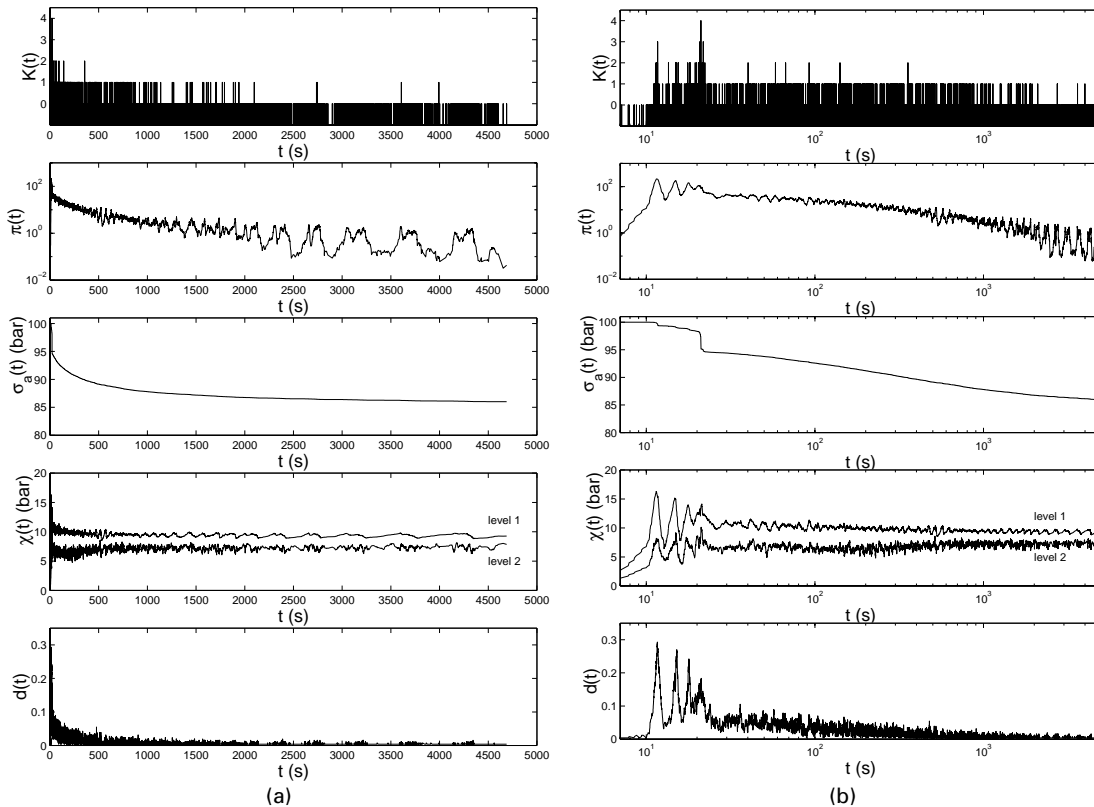

Figure 6. The reference sequence of the friction model on (a) a linear and (b) a logarithmic timescale. From top to bottom: the sequence of events, the total transition rate, the average shear stress, the standard deviation of the local shear stress, and the density of moving cells at the elementary level.
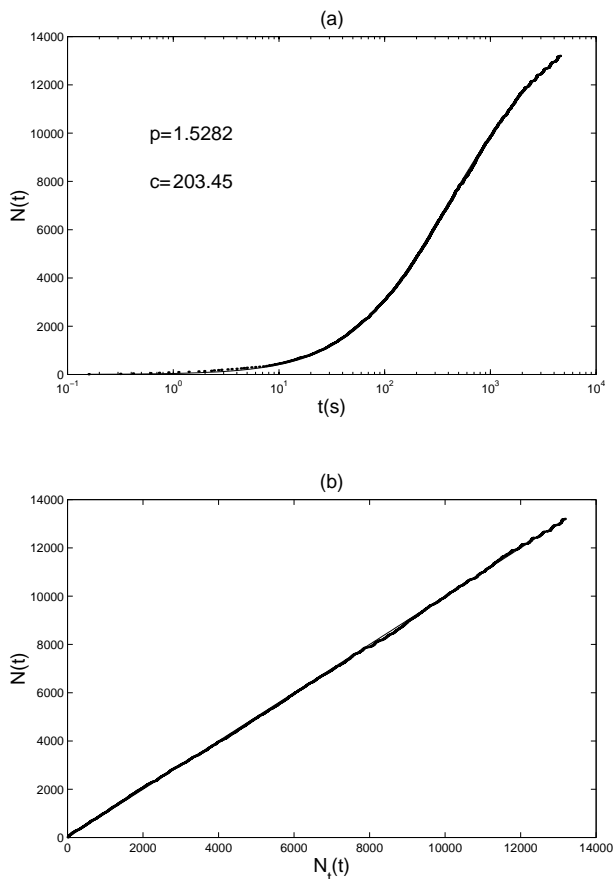
Figure 7. (a) Cumulative number of aftershocks of the reference sequence versus a logarithmic timescale and the curve representative of the modified Omori law (eq. 30). (b) Cumulative number of aftershocks of the reference sequence versus the theoretical number (straight line).

Figure 8. Magnitude–frequency law of the reference sequence: number of events (unbroken line, $b = 1.85$), number of foreshocks (dotted line, $b = 1.43$), and number of aftershocks (dashed line, $b = 2.06$) versus the hierarchical level (or magnitude; see eq. 28).

An interesting log-periodic variation of the aftershock frequency is superimposed on the trend (Fig. 11a). In Fig. 11(b) these log-periodic oscillations are seen around the theoretical straight line. This reflects the temporal distribution of the major (leading) aftershocks, which are themselves followed by a sub-sequence of aftershocks (Correig *et al.* 1997). In some cases we obtained similar behaviour for the foreshock sequences, but with only two–four oscillations (Fig. 6). Note that an attempt to test this pattern rigorously in earthquake catalogues (Gross & Rundle 1998) produced a negative result. Similarly, it is not observed in all of our numerical simulations; we have not yet been able to define the range of parameters where this pattern clearly occurs.

Let us now show how the model behaviour depends on the number of levels $\mathcal{K}$; if the scaling works properly, this dependence must be weak. Figs 12(a1), (b1) and (c1) show sequences obtained with 5, 6 and 7 levels ($\mathcal{K} = 4$, 5 and 6), retaining only the five highest levels. All the other parameters

approach this minimum of the *b*-value stems from the growth and the coalescence of old cracks, two major ingredients of the strain-softening mechanism. Coalescence at all scales (self-organization) is an intrinsic property of the SOFT rule, and no particular mechanism (e.g. pore fluid pressure) is implicitly modelled; this is an advantage (and may be a drawback) of our model.

We varied the parameters around the values of the reference sequence and found that the behaviour is unexpectedly insensitive to changes in most parameters. Except for marginal cases with no strong events or sequences of aftershocks that are too short, the system gives almost perfectly both a Gutenberg–Richter distribution of event sizes (with *b*-values for foreshocks smaller than for aftershocks) and an Omori law of the temporal aftershock decay (see Discussion, Section 5). The model appears to be the most sensitive to changes in the parameter k_b, which has the dimension of the inverse of time.

The foreshocks–main shock–aftershocks sequence can be more complex than in the reference case. Fig. 10(a) shows a main shock followed by a short sequence of aftershocks. Afterwards, during a rather long time interval, no event occurs, and, after this 'quiet' period, the aftershock sequence starts again to finally relax the system. Fig. 10(b) shows the case of several main shocks (a swarm). The case without a strong event corresponds to creep (see Fig. 13; this case is discussed below).
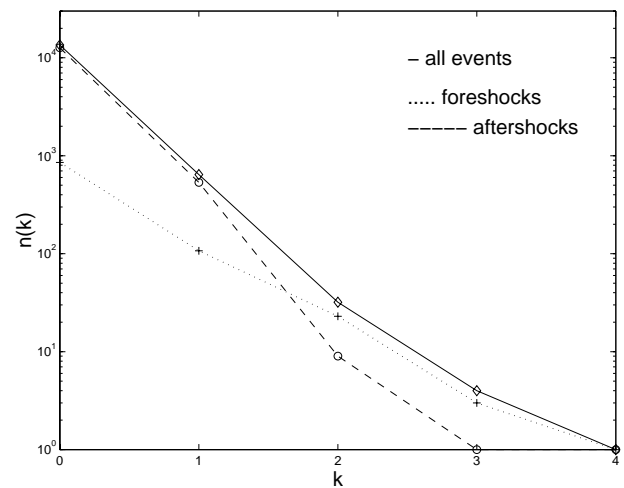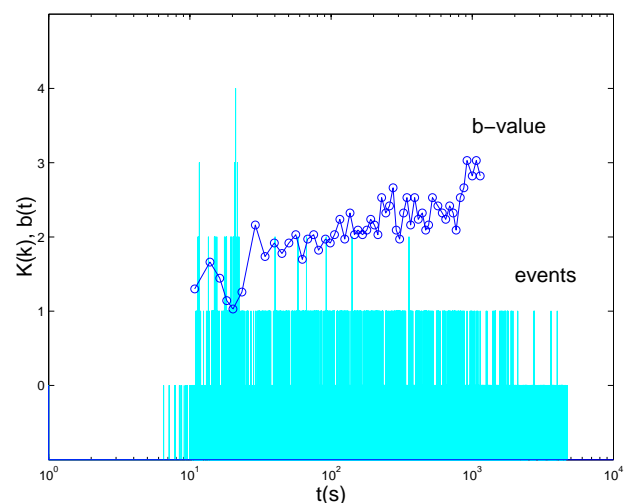
Figure 9. Evolution of the *b*-value during the reference sequence. The *b*-value is computed for consecutive time spans, each containing 200 events.
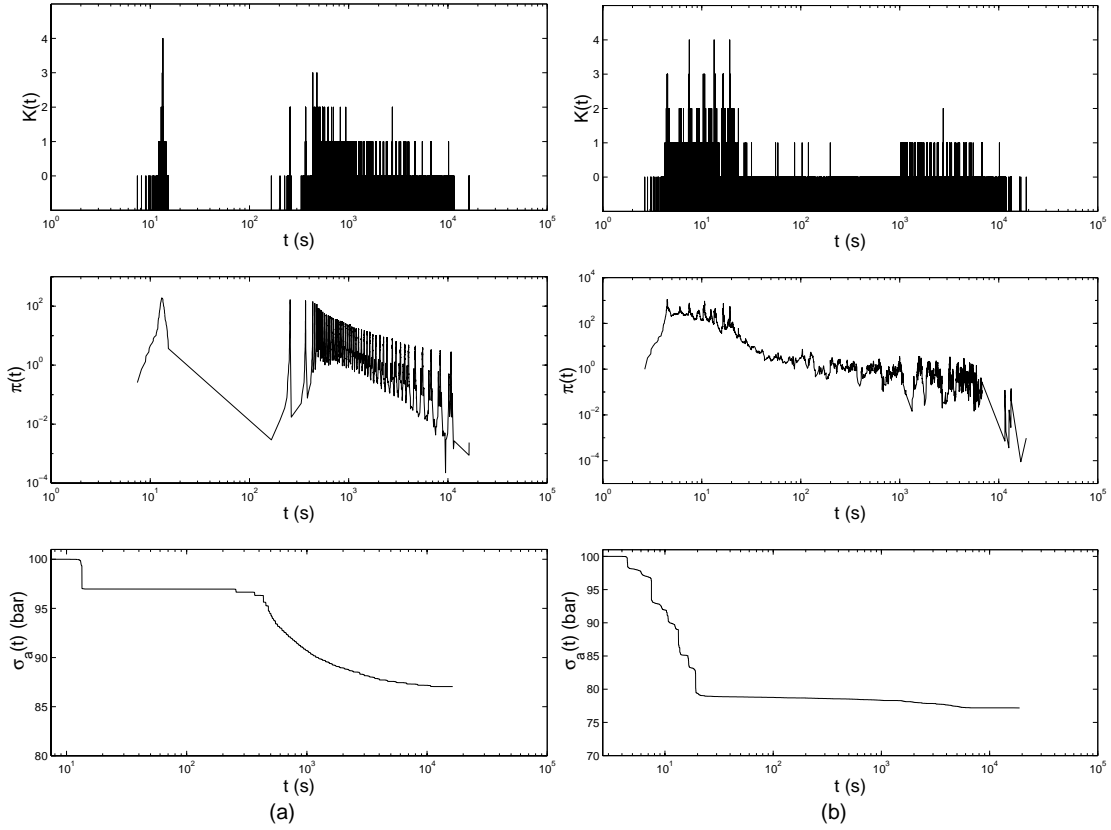
Figure 10. More complex sequences. (a) A seismic quiescence a few seconds after the main shock (same parameter values as the reference sequence except for $\theta^b = 1.5$). (b) A swarm of large earthquakes. From top to bottom on a logarithmic timescale: the event sequence, the total transition rate and the average shear stress (same parameter values as the reference sequence except for $\lambda^b = 20$ bars). Note that the modified Omori law is still respected in these two cases.

of the model are kept the same; this corresponds to systems with different spatial sizes but the same physical parameters. The sequences corresponding to the different $\mathcal{K}$ obey almost perfectly the Gutenberg–Richter law of event size distributions and the Omori law of aftershock decay. The most important difference is the duration of the power-law behaviour of the aftershock sequence as estimated by the parameter T in the Otsuka formula (eq. 31). It decreases with the number of levels (Figs 12a2, b2 and c2). This decrease of T is due to the fact that the direct cascade redistributes more stress at the lowest level for a higher value of $\mathcal{K}$. A more sophisticated rule including a redistribution of stress at all scales would increase the value of T (and make the system behaviour depend less strongly on $\mathcal{K}$).

'Friction' model with constant load. What happens after the main shock and aftershocks have passed? How does the external loading start new events? Is it possible to obtain an analogue of the seismic cycle? We understand the term 'seismic cycle' as the recurrence time (quasi-periodic or almost stochastic) of strong earthquakes, generally preceded by a growing seismic activity (foreshocks), followed by sequences of aftershocks and with a relatively aseismic behaviour between foreshocks–main shock–aftershocks sequences (Fedotov 1965; see also the detailed review in Scholz 1990). In the model described above, no strong events occur again and all the received energy is dissipated in small events; in this 'weak' system (low value of E) the dissipation keeps the average stress below the critical value (Fig. 13a). In the case of a

'strong' system (high value of E) with a high rate of external loading, the average stress can be larger than the critical value (Fig. 13b). Both cases can be interpreted as creep. However, in another 'friction' submodel derived from the present one through only a small modification, we do obtain a seismic cycle; we assume that the local stress heterogeneity is slowly decreasing with time due to some kind of 'diffusion' process, at a rate asymptotically proportional to the square root of time:

$$\sigma(C, t + \Delta t) = \sigma_a(t) + \frac{v}{\sqrt{v^2 + \Delta t \Upsilon}} (\sigma(C, t) - \sigma_a(t)), \quad (32)$$

where v is a dimensionless constant parameter, $\sigma(C, t)$ is the local shear stress in the cell C, $\sigma_a(t)$ is the average stress and Υ is a reduced diffusion coefficient (s^{-1}). Fig. 14 shows the numerical results for the set of parameters of the reference sequence except for $E = 10^{-4}$ bar s^{-1} and $\Upsilon = 10^{-4}$ s^{-1}, $v = 1$. Each peak corresponds to a foreshocks–main shock–aftershocks sequence that has the same statistical behaviour as the reference sequence.

4.4 Numerical results of the 'fracturing' model

In the 'fracturing' model, $\pi(t)$ is the total transition rate $s \rightarrow b$ and $b \rightarrow s$ at the elementary level. At higher scales, the $s \rightarrow b$ and $b \rightarrow s$ transitions are respectively associated with a seismic event or a geometric blocking. Given a slow physico-chemical healing at the lowest scale, we study the seismicity over long
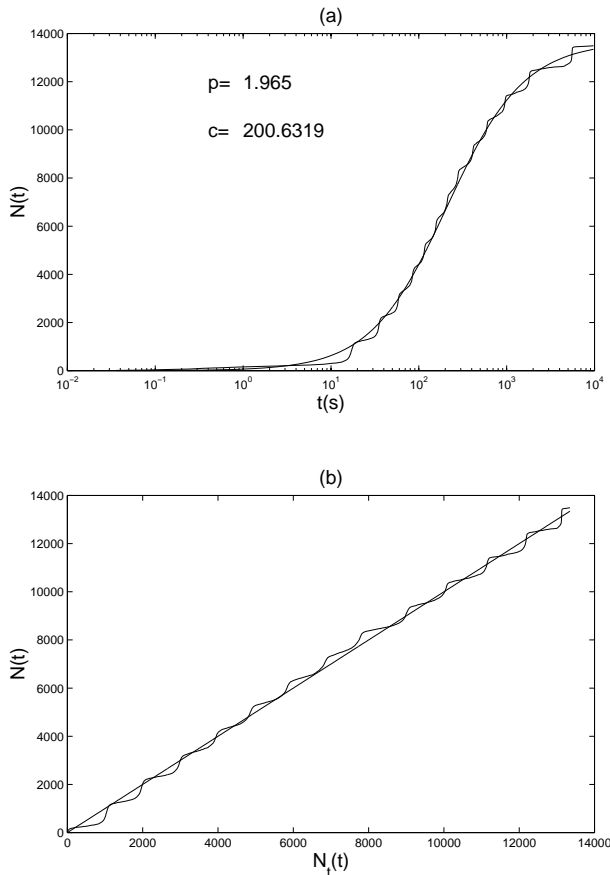
Figure 11. (a) The cumulative number of aftershocks versus time on a logarithmic scale and the curve representative of the modified Omori law (eq. 30). (b) The cumulative number of aftershocks obtained in the numerical experiment versus the theoretical experiment (straight line). Same parameter values as the reference sequence except for $\mathscr{D} = 3$.

Figure 12. Experiment with different numbers of levels: left-hand side graphs show the event sequences versus time; right-hand side graphs show the cumulative number of aftershocks versus time on a logarithmic scale and the representative curve of the Otsuka law (eq. 31) for estimated p and T parameters (same parameter values as the reference sequence except for $\lambda^b = 5$ bar).

time periods. The stress balance is between the external input and both discontinuous 'fracturing' events ($s \rightarrow b$ transition) and continuous 'friction' [broken cells C lose the excess stress $\sigma(C) - \sigma_b$ they receive from outside (E) or from internal redistribution]. We now present some typical earthquake sequences and describe the statistical behaviour of the model for different values of the parameters. The unit of time in all the figures is 10^2 s. In the captions we indicate the differences between the Table 1(a) and (b) parameter values and the those of the current numerical experiment.

4.4.1 General properties of a sequence (a realization for a given set of parameters)

Temporal distribution of earthquakes. Fig. 15 shows a typical sequence over a short time period (a time interval containing two events of the highest level). We observe several main shocks of different amplitudes—(b2) and (b3) of level 6, (b1) of level 5, (c) and (d) of level 4 and (e) of level 3. Depending on their geometrical distribution, the same number of broken cells can give events of different levels (compare a1 and a3). Comparing (a3) with (a2) shows that the average stress is correlated with the number of solid cells at the elementary level. Some main shocks have precursors (b3, c1, c2), whilst
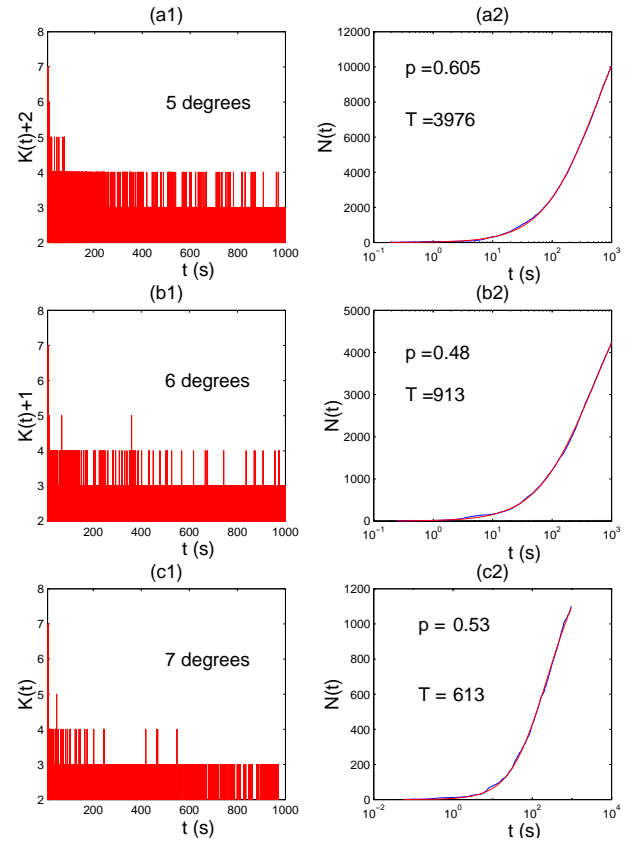
others do not (b1, b2, e). These precursors can themselves be followed by aftershocks (b3, c1). Each main shock has its own aftershock sequence. The last main shock in (b3) has a large aftershock followed by a sub-sequence of aftershocks; this large energetic release reduces the duration of the main aftershock sequence. For lower-level main shocks ($k < \mathscr{K} - 1 = 5$), due to the small number of levels ($\mathscr{K} = 6$) and the value of the scaling parameter θ (eq. 21), one observes a longer aftershock sequence duration but a smaller number of aftershocks. This long duration of the aftershock sequence is not observed for higher-level main shocks ($k > 4$); it is a consequence of the direct cascade mechanism, which redistributes all the stress drop from higher-level events directly onto the elementary level. The evolution of the average shear stress is self-similar (a2, c2, d2 and e2 have the same behaviour but on different timescales). The interseismic period between the two main shocks of the highest level (b2 and b3) is 600 yr, the duration of (e1) is 4 yr and the durations of b(1) and (b2) are 45 days. Note that the global stress drop associated with (b3) is due to a temporal seismic migration: a level 4 event triggers a level 5 event, which in turn triggers a level 6 event. Finally, in Fig. 15 there is a clear temporal clustering of events. The spatial clustering is also present: aftershocks (main shocks) occur in the neighbourhood of the main shock (foreshock), where the
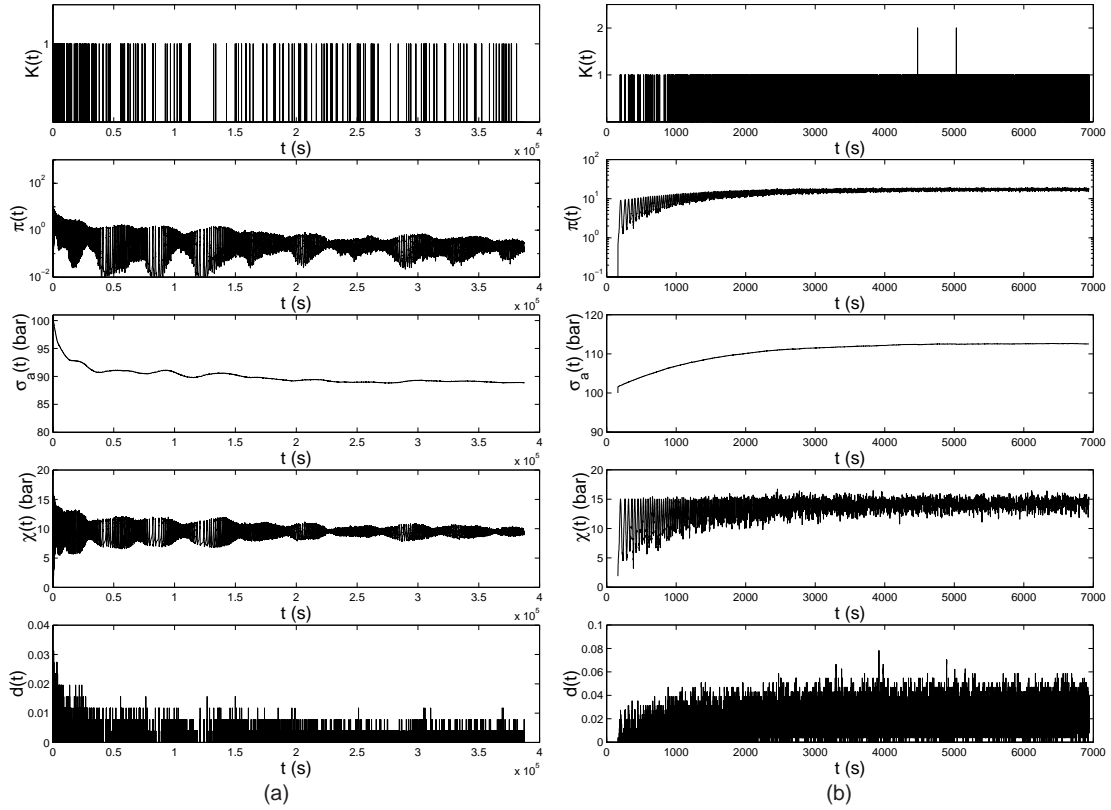
Figure 13. Examples of creep sequences. From top to bottom: the sequence of events, the total transition rate, the average shear stress, the standard deviation of the local shear stress and the density of moving cells at the elementary level. (a) The 'weak' state with $\sigma_a < \sigma_b$ (same parameter values as the reference sequence except for $E = 10^{-4}$ bar s^{-1}). (b) The 'strong' state with $\sigma_a > \sigma_b$ (same parameter values as the reference sequence except for $E = 10^{-2}$ bar s^{-1}).

redistribution of stress is positive. Given our 2-D system and the anisotropy of the critical SOFT rule, we postpone the study of the spatial distribution of our events.

Aftershocks. Fig. 16 shows a typical aftershock sequence (over 2 months) without large events (this explains the low number of aftershocks—there is no secondary sequence of aftershocks). Eq. (30) is respected (Figs 16a4 and a5), and this is the case for a large range of parameters (see below). We explain the aftershock generation mechanism as follows. The redistribution of stress rapidly increases the transition rate $s \to b$ according to eq. (9). The increase of the transition rate $b \to s$ is much slower because during the aftershock sequence this rate is inversely proportional to the number of solid cells (Fig. 16a3); in other words, just after the main shock, the 'fracturing' process is more efficient than the healing process. Later, both the local and the global stress drops (Figs 16a1 and a2) favour the decrease of the transition rate $s \to b$, whilst each fracturing event increases the transition rate $b \to s$. This balance is reached rapidly just after the main shock and more slowly later on, in agreement with the modified Omori law. The main cause of this typical $(1/(t + c)^p)$ behaviour is the heterogeneity of the stress field (Fig. 17b); in the case where an event perturbs a medium where the stress field is completely homogeneous, the decrease in aftershock frequency is exponential (Fig. 17a).

Foreshocks. Foreshocks are obviously present here: the fracturing mechanism cannot directly reach the highest level and the organization of a fracture at a given scale requires lower-scale fractures. Nevertheless, due to the history of

the fault zone, their time distribution is very complex. For studying only the distribution of foreshocks we select in our catalogues examples where earthquakes of lower amplitude precede a main shock, and we eliminate the aftershocks (i.e. all the lower-level events occurring after the higher-level event). If the medium is weakly fractured (high value of β) and the stress field is homogeneous ($\sigma_a = \sigma_s$), the foreshock activity satisfies the modified Omori law [with $t \to -t$; the typical exponent is called q instead of p (Fig. 18a)]. If the medium is not fractured (high value of β) and the stress field is heterogeneous, the foreshock activity respects the modified Omori law ($t \to -t$) with a lower value of q (Fig. 18b). If the medium is fractured (low value of β) and the stress field is heterogeneous, a main shock occurs without foreshocks and it is very difficult to isolate the foreshocks from the background seismicity.

Magnitude–frequency relation. Fig. 19 shows the magnitude–frequency relationship for a typical sequence over a very long time period (0.3 Myr). The slope of the magnitude–frequency relationship for the main shocks is smaller than the slope of the magnitude–frequency relationship for all the events, which is in turn smaller than the slope corresponding to the aftershock sequences for different levels of main shocks. The magnitude–frequency relationships for aftershock sequences of main shocks with different magnitudes do not have significantly different slopes. The b-value could easily be made closer to 1 with a more appropriate renormalization factor (see eqs 28 and 29). The slope break between levels $\mathcal{K}$ and $\mathcal{K} - 1$ is an effect of the finite domain.
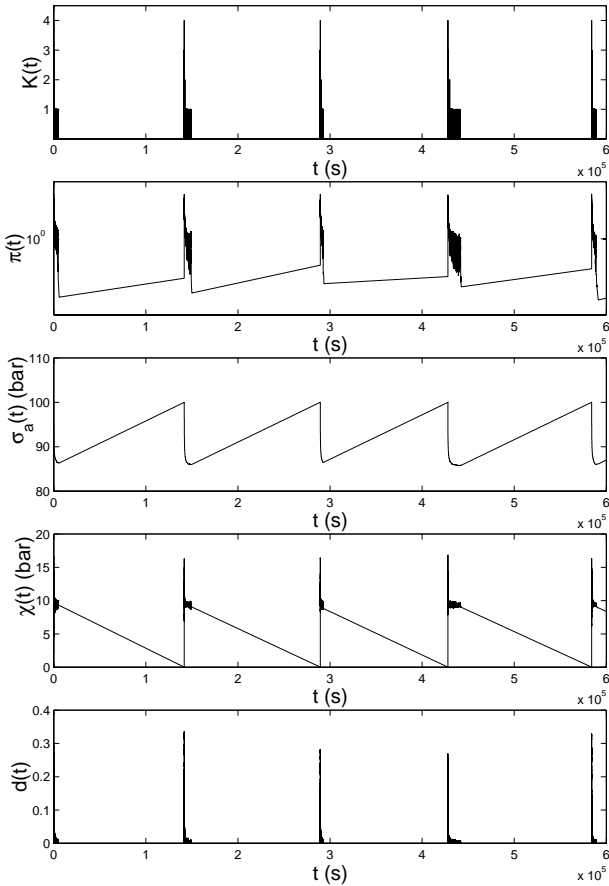
Figure 14. Examples of seismic cycles obtained with the parameter values of the reference sequence and homogenization by diffusion (see text). From top to bottom: the sequence of events, the total transition rate, the average shear stress, the standard deviation of the local shear stress and the density of moving cells.

4.4.2 Statistical properties of a set of sequences

In the following we select main shocks of level $k \geq 4$ (i.e. 4, 5 and 6), and ΔT_{aft} is adjusted for each sequence.

Aftershocks. The behaviour of the aftershock sequence essentially depends on the sharpness of the $s \to b$ transition (δ_s in eq. 9). As shown above, the aftershock sequence is due to the increase of the local shear stress resulting from the direct cascade of stress redistribution. Each aftershock modifies in turn the local shear stress in its neighbourhood; this perturbation decreases with magnitude following the scale-dependent law of parameter θ (eq. 21). Fig. 20 shows that the power-law decrease $(1/(t+c)^p)$ is still respected if $\delta_s > 2$; below this threshold value, $c/\Delta T_{aft}$ becomes too large: the global and local stress drops due to each aftershock are not large enough to decrease the $s \to b$ transition frequency, and a constant rate of aftershocks results. We observe that the p value decreases if the value of δ_s increases (Fig. 20a). The number of aftershocks and the b-value (Figs 20c and d) do not depend on δ_s.

Influence of the stress redistribution. The external loading rate E and the healing rate β are physical parameters that obviously compete. We have studied the different outputs of the model as a function of the density of fractures for different values of $E \in [10^{-9}; 10^{-4}]$ and $\beta \in [10^{-11}; 10^{-5}]$. In Figs 21, 22

and 23 each point results from a numerical simulation over a sequence of long duration ΔT ($\Delta T = 10^6 \Delta T_{aft}$).

Fig. 21(a) shows the b-value of the frequency–magnitude distribution versus the density of broken cells of the lowest level (in fact, the density average over the whole sequence duration). We observe a minimum at $d \sim 0.3$ and a plateau for a large range of $d \in [0.4; 0.7]$. The theoretical curve obtained by the integral approach has a minimum at $d_c = 0.618$, the critical value of this approach (see caption to Fig. 21). This difference in behaviour is due to the stress redistribution, which organizes the 'fracturing' process in a weakly fractured medium: the mask increases the stress in the neighbouring cells along the main direction of the cracked cells. Thus the fault zone can generate high-magnitude events even if the density of cracks is less than the critical value.

Fig. 21(b) shows the ratio $f = w_1/w_2$ between the total stress eliminated by the 'fracturing' process (through the global stress drop,

$$w_1 = \sum_k \sum_{\text{events}} \mu_2 \mathcal{R}^{3(k-\mathcal{K})} ,$$

eq. 26) and the total stress eliminated by the 'friction' process (see Section 3.2; $w_2 = E\Delta T - w_1$) versus the density of broken cells. The theoretical curve obtained from the integral approach has a maximum at the critical value of this approach. For $d > d_c$ the two modes of behaviour are similar; below this value the 'fracturing' process is more efficient for the present model with stress redistribution. The maximum value of f is reached at the value of d giving the minimum of the b-value (Fig. 21a).

The stress input during the lifetime of the broken state $(1/\beta)$. Let us now study the behaviour of our system versus E/β, which has the dimension of stress. Fig. 22 shows that some of the main system characteristics are largely controlled by this single parameter. The 'fracturing process' (Fig. 22a) is negligible if $E/\beta > 10^2$. Below this value a typical peaked behaviour is observed. We will return to this result in Section 5. The b-value versus (E/β) curve shows that b is controlled by (E/β) as long as $(E/\beta) < 10^2$ and exhibits a clear minimum (Fig. 22b). For high values of E/β, the number of high-degree events is weak and the b-value is controlled by the healing mechanism. The critical (E/β) value for which b is at a minimum can also be inferred from Fig. 22(c), whose different curves represent the densities of cracks versus E/β for different values of β; the convergence point corresponds to the critical density of cracks and the critical value of E/β. Note that this value, expressed in bars, is of the same order of magnitude as the average stress (see Table 1). A dimensional analysis could be performed in future work.

The seismic cycle. After eliminating the strong aftershocks and foreshocks, as explained previously, we noted the time intervals between two events of level $k \geq \mathcal{K} - 1$ (i.e. 5 and 6). For a minimum set of 50 time intervals, we calculated Q, the ratio of the average time interval to the standard deviation of the distribution of these time intervals. Larger values of Q reflect a more periodic behaviour. In Fig. 23(a) we show Q versus E/β for (E/β) varying from 10^{-3} to 10^3 (for lower or higher values, the high-level main shock number is too weak). A large fluctuation of Q exists, but a more periodic behaviour is observed for lower values of E/β. In Fig. 23(b), we show the b-value versus Q. An increase of the b-value is coupled with a more periodic behaviour. Such an observation is still difficult
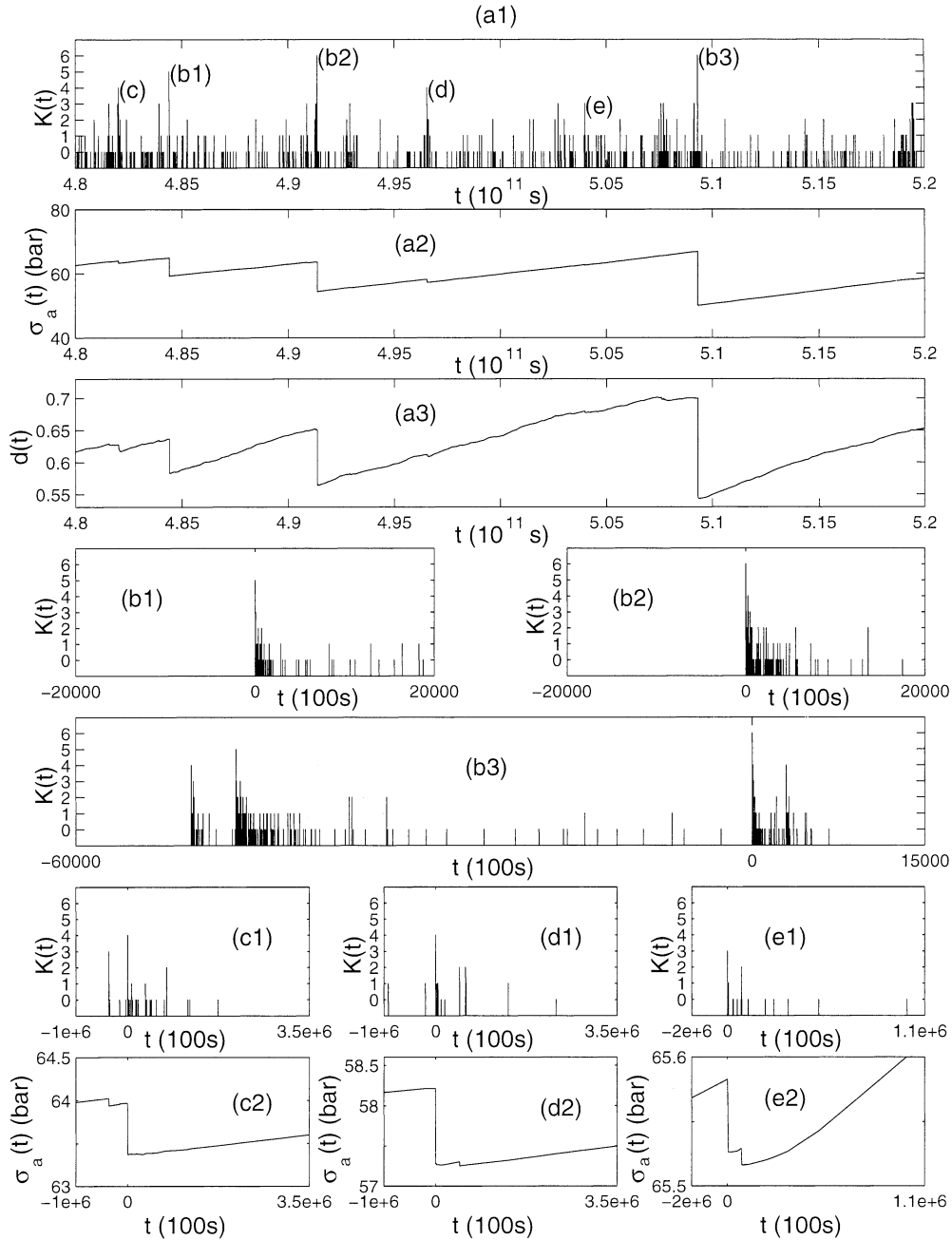
Figure 15. Intermediate sequences of earthquakes: (a1), (b1), (b2), (b3), (c1), (d1), (e1). Average shear stress versus time: (d2), (c2), (e2). Number of solid cells versus time: (a3).

5   COMPARISON WITH EXPERIMENTAL EVIDENCE: A DISCUSSION

We are aware that even a good reproduction of some regularities or empirical laws of real seismicity by a model might not be taken as strong evidence of the validity of this model. One of the reasons is that many of the regularities or empirical laws that have been claimed to have been found in

to make in real seismicity due to the short time period covered by earthquake catalogues.

the experimental evidence are controversial to various degrees, except maybe for the Gutenberg–Richter and Omori laws. However, these two very general laws do not constrain the models as strongly as might be hoped. Indeed, the Gutenberg–Richter distribution is rather easy to obtain (Allègre *et al.* 1998). Simple toy models of self-organized criticality such as a sand pile or a forest fire display a power-law distribution of the cluster sizes (Chen *et al.* 1991; Turcotte 1999). The Omori law appears more difficult to fit with model series. Nevertheless, Gutenberg–Richter and Omori laws must be observed by the model results. We note that obeying both laws
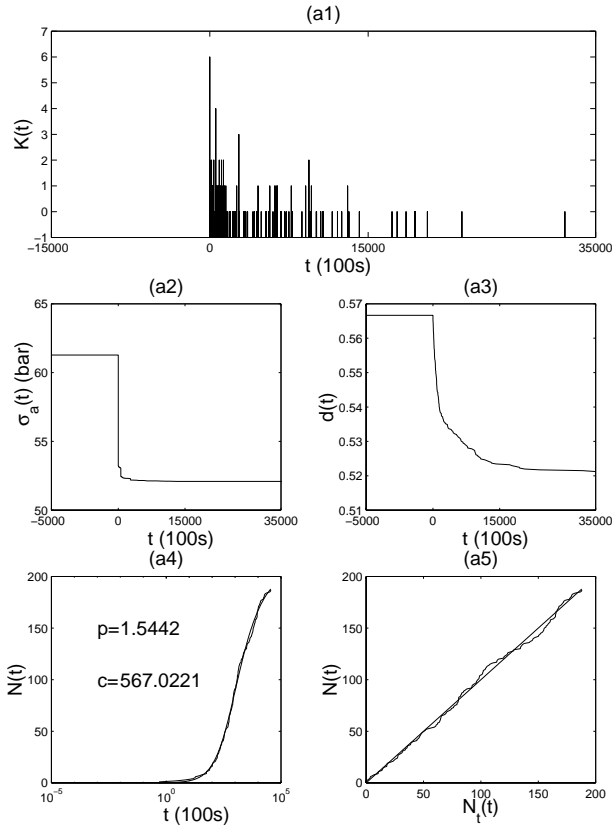
Figure 16. (a1) is a main shock–aftershock sequence. (a2) and (a3) show respectively the corresponding evolution versus time of the average stress and of the number of solid cells. (a4) shows the cumulative number of aftershocks on a logarithmic timescale and a representative curve of the modified Omori law (eq. 30). (a5) shows the cumulative number of aftershocks versus the theoretical number (straight line).

Figure 17. The cumulative number of aftershocks versus time on a logarithmic scale calculated from a critical configuration of broken cells at the elementary level (the highest-level cell is broken) and without stress redistribution ($\lambda = 0$), without healing ($\beta = 0$), without external loading ($E = 0$): (a) all the solid cells have the same local stress $\sigma_h > \sigma_s$; (b) the average stress of all the solid cells is σ_h, but, for each individual solid cell, the stress is randomly chosen in [σ_s; $\sigma_s + 2\sigma_h$]. The best-fitting curve is plotted and its formula is written [(a) gives an exponential frequency decay; (b) a ($1/(t+c)^p$) frequency decay].

simultaneously is significantly more constraining than obeying one law or the other. Comparison with more controversial observed regularities or empirical laws of seismicity must be accompanied by the required caveats. When necessary, the subdomain of parameters in which the model products and experimental evidence agree must be sketched (models in general and our own in particular have several adjustable parameters). In any case, comparing the model results with regularities or empirical laws observed in real seismicity— even these are controversial to some extent—is more efficient than comparing them with experimental evidence as a whole, without sorting. Moreover, it gives one the opportunity to explain why the model works the way it does.

We have discussed the stress pattern in the model (Sections 2.5 and 3), although little is known about the seismogenic stress in nature. In fact, we do not use in our reasoning any detailed knowledge of the stress field. We only call for a heterogeneous stress field, which results from the mechanism of multiscale redistribution of stress described in Section 2.5 and chosen for its simplicity (stress is relaxed in some cells and enhanced in neighbouring cells at all scales). An important aspect of the model is that the zone of influence where stress redistribution takes place (Fig. 4) grows proportionally to the length of the fracture. This is consistent with much of the literature on fault growth (e.g. Main 1996), but not with what happens with many
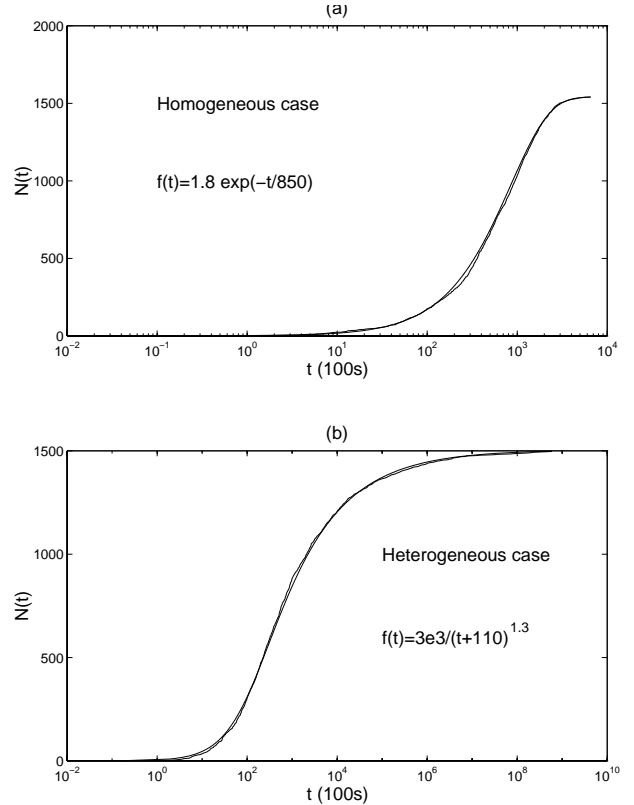
SOC models, which do not have this property since they rely on the nearest neighbour effects at small scales.

The above discussion concerns the comparison of model results with real seismicity laws (statistics on the occurrence times and magnitudes). Comparison with field tectonics is another requirement. We postpone this (ambitious) objective until we can make use of the localization properties of the model described in the present work (see the next section).

6 CONCLUSIONS AND PERSPECTIVES

The new approach presented here, with a direct simulation of the stress redistribution, is an extension of the previous SOFT model. We have now built a numerical laboratory that will allow a large number of experiments characterized by different timescales, from the dynamics of the rupture ('friction' submodel) to the history of a fault zone ('fracturing' submodel). Our present modelling produces a large range of observed seismic sequences with a precise temporal (and spatial) location of events.

The multiple-scale approach coupled with the SOFT rule with memory has allowed us to incorporate the major components of brittle fracture: healing of cracks, increase in micro-crack density, rupture threshold, heterogeneity of the stress field
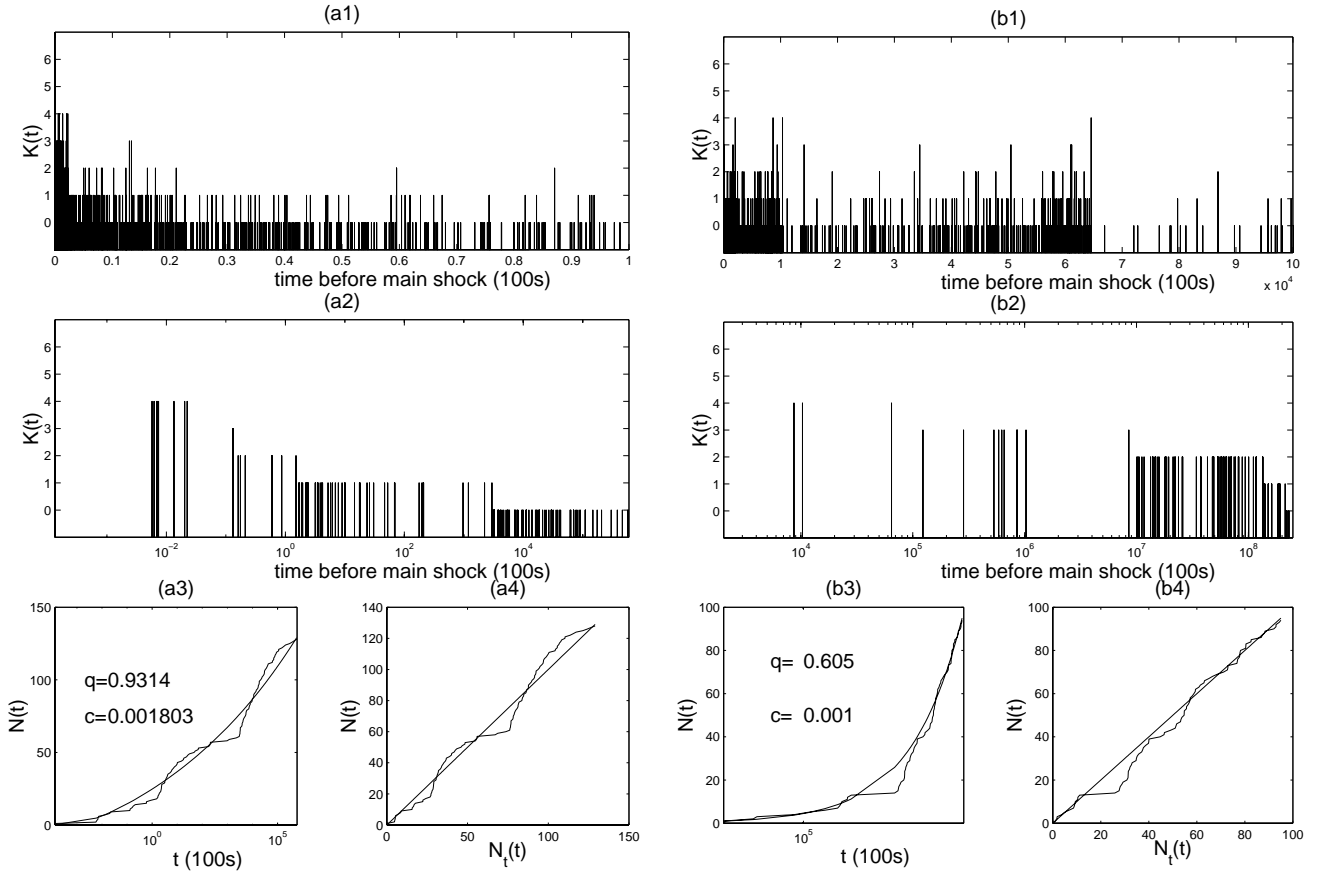
Figure 18. (a1), b(1) Example of complete foreshock sequences with a linear timescale (parameter value set of Tables 1a and b with different initial conditions; see text). (a2), (b2) The sequences of the selected foreshocks on a logarithmic timescale. (a3), (b3) The cumulative number of foreshocks on a logarithmic timescale and a theoretical estimate from the modified Omori law (eq. 30). (a4), (b4) The cumulative number of foreshocks versus the theoretical number (straight line).

and propagation of fractures. Incorporating these properties in our abstract modelling gives rise to a large number of complex types of behaviour that can be related to the complexity of real earthquakes. The simplicity of the model is an advantage in better understanding the physical origin of the complexity of the behaviour. The statistical properties of our system have been studied, even though the main goal of the present paper was to reproduce the spatio-temporal clustering of earthquakes.

We have shown that the $1/(t+c)^p$ behaviour of the aftershock frequency is a direct expression of the heterogeneous stress distribution at the main shock time (see Sections 4.3 and 4.4). This conclusion is valid for both submodels since the mechanism of stress redistribution is the same. In real earthquakes, aftershocks are present in most cases and the variation of p can be analysed as a function of the heterogeneity of the stress distribution.

The physics of the healing (physico-chemical process or geometrical blocking) has to be taken into account in a fault zone. The ratio (E/β) between the external loading rate and the healing appears to be a general control parameter. The value of this parameter discriminates between the domains of applicability of the two submodels. The foreshock activity during the long time period preceding an earthquake depends strongly on E/β. If this rate is high, an increase in seismicity is observed before the main shock, and foreshocks obviously occur; the unstable state is reached through the fracturing of the solid

parts of the medium. On the other hand, with a low healing rate the system always stays in an unstable state around a critical distribution of cracks, and the foreshock activity is random.

The relative density and the distribution (structural heterogeneity) of the solid parts of the medium on the one hand favour the loading of the shear stress, which can be eliminated by earthquakes, and on the other hand control the dimension of the largest earthquake that can occur in a fault zone.

A quasi-periodic seismic cycle is obtained in both submodels when the stress field becomes quasi-homogeneous during the loading period (interseismic phase). In the case of the 'fracturing' submodel, the periodic character of the seismic cycle is enhanced when the *b*-value increases.

There are many points that we intend to tackle in the future. We have to develop systematic studies of the statistical properties of our system and determine the origin of their variations. To understand the mechanism that leads to the main shock, and to decide whether or not this mechanism is different from the relaxation process, we have to study how the distribution of the stress field influences the increase in foreshock activity. The relative density of the main shocks with precursors has to be evaluated, and we will try to draw a phase diagram representing the different types of seismic processes: creep, swarms of small earthquakes, and earthquakes with or without precursors. We will try to develop the relation-
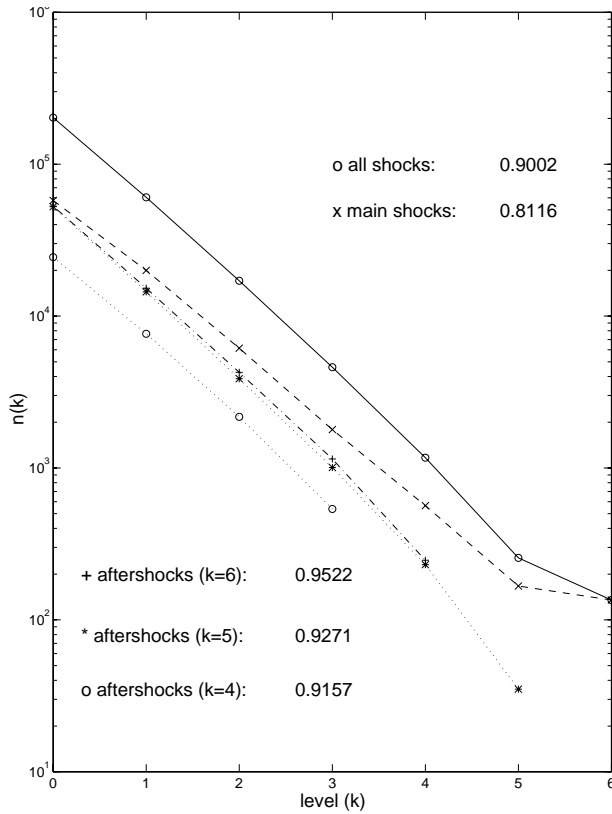
Figure 19. The magnitude–frequency relationship for all events (solid line), for main shocks only (dashed line), for aftershocks of main shocks of level $\mathcal{K}$ (dot-dashed line) and for aftershocks of main shocks of level $\mathcal{K}-1$ and $\mathcal{K}-2$ (dotted lines). Calculated b-value are indicated.

Figure 20. (a) The average value and standard deviation of the parameter p of eq. (30) compiled from a large number of aftershock sequences ($\sim 10^3$; we run the model for a very long time to get this large number) versus δ_s. (b) The average value of the parameter c of eq. (30) versus δ_s. (c) The average number of aftershocks and the standard deviation of this number versus δ_s. (d) The average b-value versus δ_s.

ship between these seismic processes and, for example, the parameters of the friction and fracturing laws (eqs 9 and 12) (as done here for the aftershock frequency decay as a function of δ_s). We will also pay careful attention to the particular case of earthquake triggering.

We will also consider a 3-D hierarchical model with a tensorial stress field rather than a scalar one, and interactions between cracks of different orientations (e.g. following Allègre & Le Mouël 1994). It will be possible to compare our synthetic catalogues—containing both times and locations—with real data and in turn to constrain our physical parameters. This stage is of course the most important from the geophysical point of view. We have to interact with rock mechanicists to incorporate in our model more realistic ingredients for the rupture propagation and to develop a fragility criterion in the static (nucleation) or dynamic case (growth). It will be possible to calculate synthetic seismograms of large events taking into account the history of the rupture. It will also be important to refine the mechanism of the stress redistribution during the relatively short time period following an event and its relation with the aftershocks activity and the heterogeneity of the stress field. With our multiple-scale approach we will try to answer the following questions: how can an *a priori* heterogeneous stress field at the smallest scale produce major ruptures accommodating the global tectonic stress field (introduced at the highest scale), and how does the system redistribute this global tectonic stress field at smaller scales?
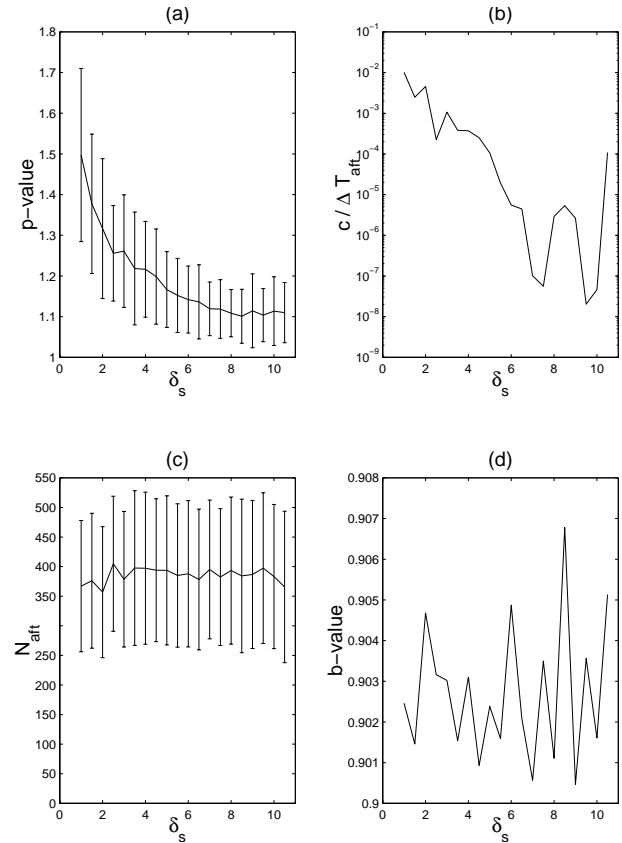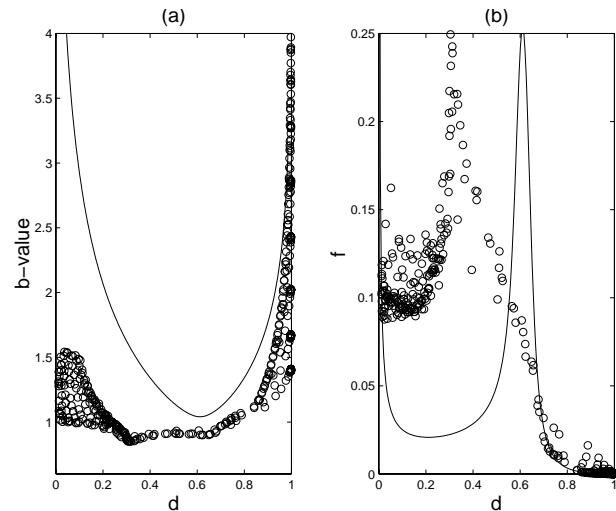

Figure 21. Evolution of (a) the b-value and (b) the f-value (see text) versus the average density of fractures at the lowest level. Open circles are from numerical experiments with different values of E and β (see text), while the solid line is calculated from the integral approach [if f_l and d_l are respectively the event frequency and the crack density at level l, the event frequency at the higher level is $f_{l+1}=f_l(1-d_{l+1})(1-(1-d_l^2)^2)$].
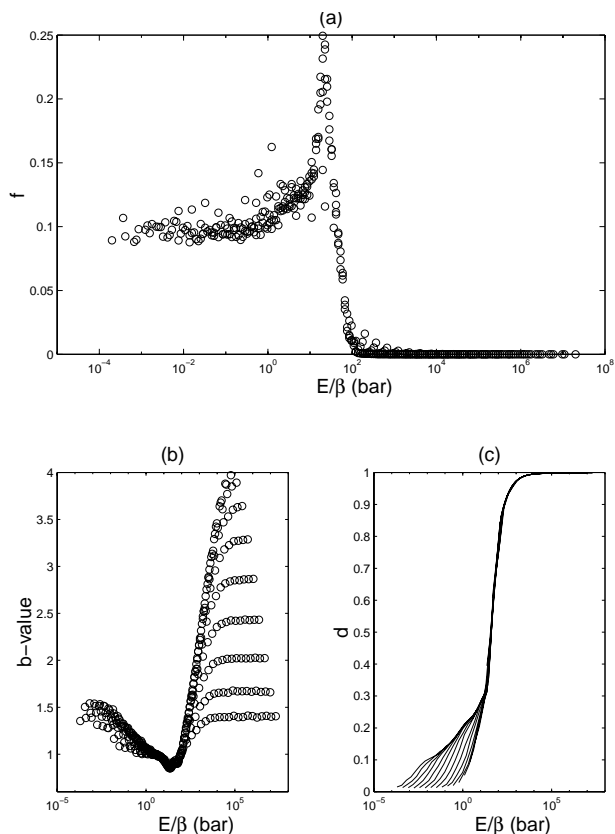
Figure 22. Evolution versus E/β of (a) f, the ratio between the total (over the entire sequence) stress dissipated by the 'fracturing' process and the total stress dissipated by the 'friction' process, (b) the *b*-value and (c) the density of fractures at the lowest level.
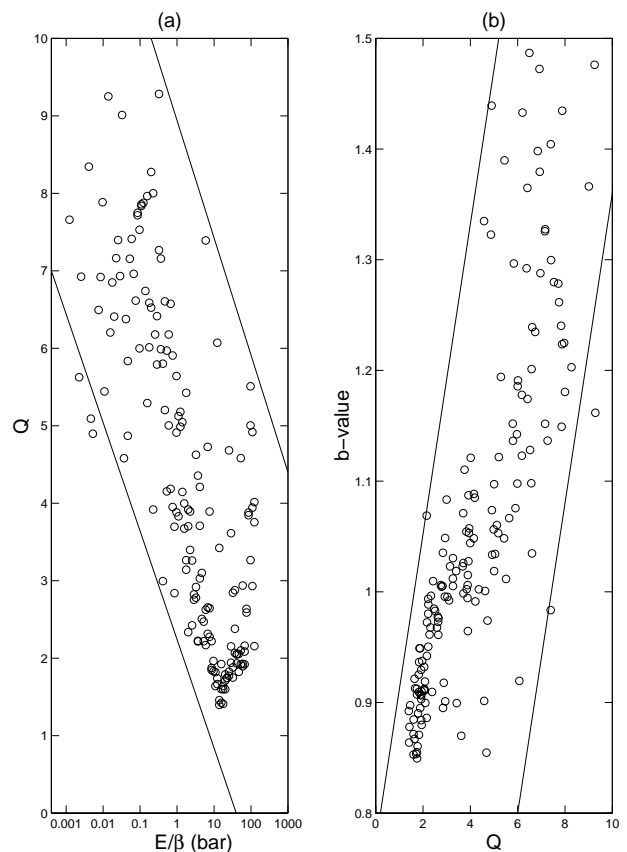

Figure 23. (a) Evolution of parameter Q versus E/β. (b) Evolution of the *b*-value versus Q.

133The geology of any area is obviously heterogeneous. Introducing a 3-D fault zone model with pre-existing geological structures is a promising perspective. In the domain of the fault zone where an event takes place, the system will not only receive a constant rate of potential elastic energy but also an unsteady rate through the interaction with the neighbouring fault systems (see the multidomain approach of Allègre *et al.* 1995). This can be done in the framework of a 3-D rupture process, where our multiple-scale approach constitutes a necessary simplification.

ACKNOWLEDGMENTS

REFERENCES

Aki, K., 1984. Asperities, barriers, characteristic earthquakes and strong motion prediction, *J. geophys. Res.,* **86,** 5867–5872.

Allègre, C.J. & Le Mouël, J.L., 1994. Introduction of scaling techniques in brittle fracture of rocks, *Phys. Earth planet. Inter.,* **87,** 85–93.

Allègre, C.J., Le Mouël, J.L. & Provost, A., 1982. Scaling rules in rock fracture and possible implications for earthquake prediction, *Nature,* **297,** 47–49.

Allègre, C.J., Le Mouël, J.L., Chau, H.D. & Narteau, C., 1995. Scaling organization of fracture tectonics (SOFT) and earthquake mechanism, *Phys. Earth planet. Inter.,* **92,** 215–233.

Allègre, C.J., Shebalin, P., Le Mouël, J.L. & Narteau, C. 1998. Energetic balance in scaling organization of fracture tectonics, *Phys. Earth planet. Inter.,* **106,** 139–153.

Bak, P. & Tang, C., 1989. Earthquakes as a self-organized critical phenomenon, *J. geophys. Res.,* **94,** 15 635–15 637.

Båth, M., 1974. *Spectral Analysis in Geophysics,* Elsevier, Amsterdam.

Ben-Zion, Y., 1996. Stress, slip and earthquakes in models of complex single-fault systems incorporating brittle and creep deformations, *J. geophys. Res.,* **101,** 5677–5706.

Binney, J.J., Dowrick, N.J., Fisher, A.J. & Newman, M.E.J., 1992. *The Theory of Critical Phenomena, an Introduction to the Renormalization Group,* Clarendon Press, Oxford.

Blanter, E.M., Shnirman, M.G. & Le Mouël, J.L., 1997. Hierarchical model of seismicity: scaling and predictability, *Phys. Earth planet. Inter.,* **103,** 135–150.

Brune, J.N., 1968. Seismic moment, seismicity and rate along major fault zones, *J. geophys. Res.,* **73,** 777–784.

Burridge, R. & Knopoff, L. 1967. Model and theoretical seismicity, *Bull. seism. Soc. Am.,* **57,** 341–371.

Campillo, M. & Ionescu, I.R., 1997. Initiation of antiplane shear instability under slip dependent friction, *J. geophys. Res.,* **102,** 20 263–20 271.

Chen, K., Bak, P. & Obukhov, S.P., 1991. Self-organized criticality in a crack-propagation model of earthquakes, *Phys. Rev. A,* **43,** 625–630.

Cochard, A. & Madariaga, R., 1994. Dynamic faulting under rate-dependent frictions, *Pure appl. Geophys.,* **142,** 419–445.

Correig, A.M., Urquizú, M. & Vila, J., 1997. Aftershock series of event February 18, 1996: an interpretation in terms of self-organized criticality, *J. geophys. Res.,* **102,** 407–427.

Dieterich, J., 1979. Modeling of rock friction: 1. Experimental results and constitutive equations, *J. geophys. Res.,* **84,** 2161–2168.

Dieterich, J., 1994. A constitutive law for rate of earthquake production and its application to earthquake clustering, *J. geophys. Res.,* **99,** 2601–2618.

Dubois, J. & Gvishiani, A., 1998. *Dynamic Systems and Dynamic Classification Problems in Geophysical Applications,* Springer, Berlin.

Ellsworth, W.L. & Beroza, G.C., 1995. Seismic evidence for an earthquake nucleation phase, *Nature,* **268,** 851–854.

Fedotov, S.A., 1965. Regularities in the distribution of strong earthquakes in Kamchatka, the Kuriles, and Northern Japan, *Akad. Nauk USSR. Inst. Fiz. Zeml.,* **36,** 66–95.

Gross, S. & Rundle, J., 1998. A systematic test of time-to-failure analysis, *Geophys. J. Int.,* **133,** 57–64.

Gutenberg, B. & Richter, C., 1944. Frequency of earthquakes in California, *Bull. seism. Soc. Am.,* **34,** 185–188.

Hainzl, S., Zöller, G. & Kurths, J. 1999. Similar power-laws for fore- and aftershock sequences in a spring-block model of earthquakes, *J. geophys. Res.,* **104,** 7243–7254.

Harris, R.A., 1998. Introduction to special section: stress triggers, stress shadows, and implications for seismic hazard, *J. geophys. Res.,* **103,** 24 347–24 358.

Kanamori, H. & Anderson, D.L. 1975. Theoretical basis of some empirical relations in seismology, *Bull. seism. Soc. Am.,* **65,** 1073–1095.

King, G., 1983. The accommodation of large strain in the upper lithosphere of the Earth and other solids by self similar fault systems, *Pure appl. Geophys.,* **121,** 761–815.

Knopoff, L., 1997. The physics of earthquakes, in *Fourth Workshop on Non-linear Dynamics and Earthquake Prediction,* Trieste, Italy.

Kostrov, V.V., 1974. Seismic moment and energy of earthquakes, and seismic flow of rocks, *Phys. Sol. Earth,* **1,** 23–44.

Kulldorf, G., 1961. *Contribution to the Theory of Estimation Rank Grouped and Partially Grouped Samples,* Almquist & Wiksell, Stockholm.

Lee, W.H.K., 1997. *Algorithms for Earthquake Statistics and Prediction,* IASPEI Software Library.

Main, I.G., 1996. Statistical physics, seismogenic, and seismic hazard, *Rev. Geophys.,* **34,** 433–462.

Main, I.G., 1997. Long odds on prediction, *Nature,* **385,** 19–20.

Main, I.G., Meredith, P.G., Sammonds, P.R. & Jones, C., 1990. Influence of fractal flaw distribution on rock deformation in the brittle field, *Geol. Soc. Lond. Spec. Publ.,* **54,** 81–96.

Marrone, C., 1998. The effect of loading rate on static friction and the rate of fault healing during the earthquake cycle, *Nature,* **391,** 69–72.

Marrone, C. & Scholz, C.H., 1988. The depth of seismic faulting and the upper transition from stable to unstable slip regimes, *Geophys. Res. Lett.,* **15,** 621–624.

Molchan, G., Kronrod, T. & Panza, G., 1997. Multi-scale seismicity model for seismic risk, *Bull. seism. Soc. Am.,* **87,** 1220–1229.

Okada, Y., 1985. Surface deformation due to the shear and tensile faults in a half space, *Bull. seism. Soc. Am.,* **75,** 1135–1154.

Okada, Y., 1992. Internal deformation due to shear and tensile faults in a half-space, *Bull. seism. Soc. Am.,* **82,** 1018–1040.

Omori, F., 1894, On after-shocks of earthquakes, *J. Coll. Sci. Imp. Univ. Tokyo,* **7,** 111–200.

Otsuka, M., 1985. Physical interpretation of Omori's formula, *Sci. Rep. Shimabara Earthq. Volc. Obs.,* **13,** 11–20.

Papazachos, B., 1975. Foreshocks and earthquake prediction, *Tectonophysics,* **28,** 213–226.

Rice, J.R. & Ben-Zion, Y., 1996. Slip complexity in earthquake faults models, *Proc. Nat. Acad. Sci. USA,* **931,** 3811–3818.

Sammonds, P.R., Meredith, P.G. & Main, I.G., 1992. Role of pore fluids in the generation of seismic precursors to shear fracture, *Nature,* **359,** 228–230.

Scholz, C.H., 1990. *The Mechanism of Earthquakes and Faulting,* Cambridge University Press, Cambridge.

Scholz, C.H., 1998. Earthquakes and friction laws, *Nature,* **391,** 37–41.

Shnirman, M.G. & Blanter, E.M., 1999. Mixed hierarchical model of seismicity: scaling and prediction, *Phys. Earth planet. Inter.,* **111,** 295–303.

Smith, W.D., 1981. The *b*-value as an earthquake precursor, *Nature,* **289,** 136–139.

Tapponnier, P. & Brace, W.F., 1976. Development of stress-induced microcracks in Westerly granite, *Mech. Min. Sci. Geomech. Abstr.,* **131,** 103–112.

Tse, S. & Rice, J., 1986. Crustal earthquake instability in relation to the depth variation of friction slip properties, *J. geophys. Res.,* **915,** 9452–9472.

Turcotte, D.L., 1999. Seismicity and self-organized criticality, *Phys. Earth planet. Inter.,* **111,** 275–293.

Utsu, T., Ogata, Y. & Matsu'ura, R., 1995. The centenary of the Omori formula for a decay law of aftershocks activity, *J. Phys. Earth,* **43,** 1–33.

Yamashita, T. & Ohnaka, M., 1991. Nucleation process of unstable rupture in the brittle regime: a theoretical approach based on experimentally inferred relations, *J. geophys. Res.,* **96,** 8351–8367.